

Original contains color  
plates. All drawings  
and text will be in black and  
white

AD-A255 277



(2)

CONTRACT NO.: DAMD17-90-Z-0054

DTIC  
ELECTE  
SEP 18 1992  
S C D

TITLE: Training, Muscle Fatigue and Stress Fractures

PRINCIPAL INVESTIGATOR: Clinton T. Rubin

P.I. ADDRESS: Musculo-Skeletal Research Laboratory  
Department of Orthopaedics  
Health Sciences Center T18-030  
State University of New York  
Stony Brook, New York 11794-8181

DATE OF REPORT: July 29, 1992

TYPE OF REPORT: Final Report

PREPARED FOR: U.S. Army Medical Research and Development Command  
Fort Detrick  
Frederick, Maryland 21702-5012

DISTRIBUTION STATEMENT: Approved for public release;  
distribution unlimited

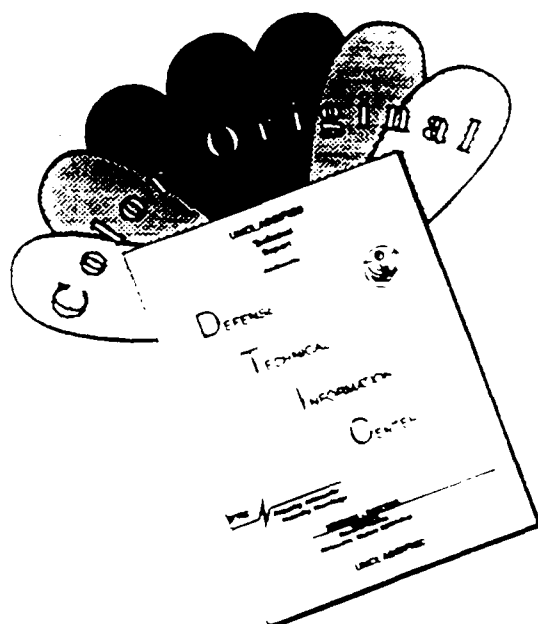
92 9 17 005

415 312

92-25383



# DISCLAIMER NOTICE



THIS DOCUMENT IS BEST QUALITY AVAILABLE. THE COPY FURNISHED TO DTIC CONTAINED A SIGNIFICANT NUMBER OF COLOR PAGES WHICH DO NOT REPRODUCE LEGIBLY ON BLACK AND WHITE MICROFICHE.

REPORT DOCUMENTATION PAGE			Form Approved OMB No 0704-0188	
<small>Public reporting burden for this collection of information is estimated to average 1 hour per response, including the time for reviewing instructions, searching existing data sources, gathering and maintaining the data needed, and completing and reviewing the collection of information. Send comments regarding this burden estimate or any other aspect of this collection of information, including suggestions for reducing this burden, to Washington Headquarters Services, Directorate for Information Operations and Reports, 1215 Jefferson Davis Highway, Suite 1204, Arlington, VA 22202-4302, and to the Office of Management and Budget, Paperwork Reduction Project (0704-0188), Washington, DC 20503.</small>				
1. AGENCY USE ONLY (Leave blank)		2. REPORT DATE July 29, 1992	3. REPORT TYPE AND DATES COVERED Final 28 Sep 90 - 29 Dec 91	
4. TITLE AND SUBTITLE Training, Muscle Fatigue and Stress Fractures			5. FUNDING NUMBERS  DAMD17-90-Z-0054  61102A 30161102BS15 CA DA335568	
6. AUTHOR(S)  Clinton T. Rubin				
7. PERFORMING ORGANIZATION NAME(S) AND ADDRESS(ES) Musculo-Skeletal Research Laboratory Department of Orthopaedics Health Sciences Center T18-030 State University of New York Stony Brook, New York 11794-8181			8. PERFORMING ORGANIZATION REPORT NUMBER	
9. SPONSORING / MONITORING AGENCY NAME(S) AND ADDRESS(ES) U.S. Army Medical Research & Development Command Fort Detrick Frederick, Maryland 21702-5012			10. SPONSORING / MONITORING AGENCY REPORT NUMBER	
11. SUPPLEMENTARY NOTES				
12a. DISTRIBUTION AVAILABILITY STATEMENT  Approved for public release; distribution unlimited			12b. DISTRIBUTION CODE	
13. ABSTRACT (Maximum 200 words)  Abstract on page 3 of report.				
14. SUBJECT TERMS  RA 3, Stress fracture; Bone remodeling; Strain; Stress reaction			15. NUMBER OF PAGES	
			16. PRICE CODE	
17. SECURITY CLASSIFICATION OF REPORT  Unclassified	18. SECURITY CLASSIFICATION OF THIS PAGE  Unclassified	19. SECURITY CLASSIFICATION OF ABSTRACT  Unclassified	20. LIMITATION OF ABSTRACT  Unlimited	

FOREWORD

Opinions, interpretations, conclusions and recommendations are those of the author and are not necessarily endorsed by the U.S. Army.

✓  
Where copyrighted material is quoted, permission has been obtained to use such material.


✓  
Where material from documents designated for limited distribution is quoted, permission has been obtained to use the material.

✓  
Citations of commercial organizations and trade names in this report do not constitute an official Department of the Army endorsement or approval of the products or services of these organizations.

✓  
In conducting research using animals, the investigator(s) adhered to the "Guide for the Care and Use of Laboratory Animals," prepared by the Committee on Care and Use of Laboratory Animals of the Institute of Laboratory Animal Resources, National Research Council (NRC Publication No. 86-23, Revised 1985).

✓  
For the protection of human subjects, the investigator(s) have adhered to policies of applicable Federal Law 45 CFR 46.

✓  
In conducting research utilizing recombinant DNA technology, the investigator(s) adhered to current guidelines promulgated by the National Institutes of Health.

  
PI Signature

7-29-92  
Date

CONUS  
JUL 90

Final Report

for work performed on Army Contract #DAMD17-90-Z-0054 entitled:

**Training, Muscle Fatigue and Stress Fractures**

over the period of

November 1990 - June 1992

Investigators:

Clinton Rubin, Ph.D., Ted Gross, M.S., Farshid Guilak, Ph.D., Yi-Xian Qin, M.S.,

Henry J. Donahue, Ph.D., Carol Mase, D.V.M., & Kenneth McLeod, Ph.D.

Musculo-Skeletal Research Laboratory  
Department of Orthopaedics  
State University of New York  
Stony Brook, New York 11794-8181

COTR:

Lt. Col. Bruce Jones, M.D.  
Exercise Physiology Division  
U.S.A.R.I.E.M.  
Natick, Massachusetts 01760

DTIC QUALITY INSPECTED 5

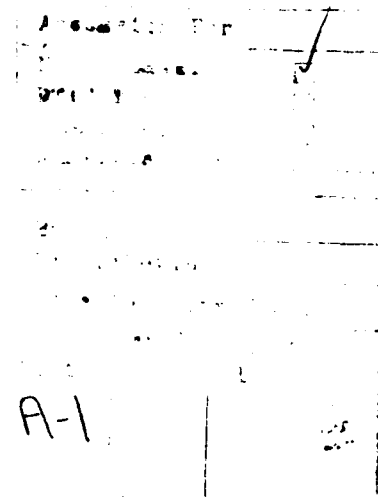


## Table of Contents

Front Cover	i
Report Documentation Page	ii
Foreword	iii
Title Page	1
Abstract	3
Contract Synopsis	4
Military Implications	4
Introduction	5
Military Significance	7
Overview of Previous Results	8
<i>a. Changes in the distribution of strain concurrent to metabolic fatigue</i>	
<i>b. Skeletal remodeling response to excessive repetitive loading</i>	
<i>c. Correlation of animal models to human pathology</i>	
Experimental Design and Methods	15
<i>a. Measurement of bone strains in vivo</i>	
<i>b. Functional isolation of the ulna</i>	
<i>c. Dynamic loading of the isolated ulna preparation</i>	
<i>d. Histology</i>	
<i>e. Microradiography</i>	
<i>f. Areal analysis</i>	
Final Results of Current Contract	24
<i>a. Defining the applied strain state of the turkey ulna model</i>	
<i>b. Formation of the finite element model</i>	
<i>c. Differential response of bone to axial and torsional loading</i>	
Discussion	38
Conclusions	40
References	41

### Abstract

The objective of this twenty month contract has been to identify the causative mechanical factors responsible for the stress fracture lesion. Over this period, the research has focussed exclusively on an animal model developed specifically for this work, the functionally isolated avian ulna. The stress fracture protocols have exploited this model's ability to withstand, *in vivo*, high cyclic loading, applied both axially and torsionally, with the aim of identifying that specific mechanical agent within the physical regimen which stimulates this debilitating condition.

Previous work from our group suggests that the lesion is a product of tissue remodeling (intracortical porosis), *not* material microdamage. As importantly, the site of the lesion, when correlated to the mechanical environment to which the bone is subjected, emphasizes that the pathology predominates in areas of *least* normal strain, *not* those areas subject to greatest deformation. Finally, the pathology observed in this animal model is identical to that which occurs in humans, demonstrating the appropriateness of using these studies to better understand the etiology of the human condition. From these developments, we proposed that the stress fracture lesions, or rather elevated intracortical remodeling, was not intensity dependent, but instead was a product of redundant, cyclic activity.

The experiments funded by this current contract further support the suggestion that the lesion is generated by some factor other than material failure. Indeed, from the data analyzed in these protocols, it appears that the stress fracture lesion is *not* caused by the amplitude of the strain, but rather by the number of cycles to which the bone is subjected. Bone subjected to 5000 cycles per day of an extremely low level of peak longitudinal normal (axially oriented) strain (1000 microstrain) caused elevated intracortical remodeling to the point the bone appeared moth-eaten. The number of intracortical porosities increased by seven times over control, while the mean area of bone resorbed from the cortex over the four week period rose from 0.20mm<sup>2</sup> in control to 1.39mm<sup>2</sup> in the axially loaded bones. Again, the highest level of intracortical activity occurred in the area of least strain. In stark contrast to the intracortical pathology resulting from axial loading, when the bone was subject to shear rather than normal strain, thus avoiding the focal areas of low strain energy density, essentially eliminated intracortical remodeling. Neither the number of intracortical events nor the amount of bone lost from the cortex was significantly different from control. This differential response suggests the bone has the ability to distinguish these two types of strain, and indeed initiate two distinct remodeling responses. Finally, counter to our original hypothesis, *combining* normal and shear strain did *not* extinguish the intracortical remodeling. The intracortical remodeling and event number was not significantly different from the purely axially loaded case. However, this combined loading did appear to *amplify* the consequences of the intracortical pathology. The porosities stimulated by the normal strain first weakened the structure, with the subsequent torsional loads causing frank failure in several of the experimental preparations.

This work has provided unique and critical insight to the pathogenesis of the stress fracture lesion. This information holds direct and immediate impact on elucidating the cause of the military's greatest loss of recruit time. Unfortunately, due to premature termination of funding of this contract, the work to identify the causal agent of the lesion

must be halted. However, it is hoped that this basic science work, at the very least, illustrates that the general dogma for stress fracture lesion pathogenesis is not well supported. Indeed, the stress fracture lesion is *not* a fatigue failure of the bone material, but rather an elaborate - but poorly understood - biologic response of the bone tissue to high cyclic loading.

#### **Contract Synopsis**

Subjecting a bone to high cycle numbers of low normal strain will elevate intracortical porosis, thereby compromising the structure's ability to withstand loading from other directions (e.g. torsion). However, even at high cycle numbers, shear strain does *not* stimulate remodeling, and therefore did not contribute to the appearance of the lesion. Nonetheless, it would appear that combined activity is exceedingly dangerous, as the skeletal structure is at first weakened by the porosities stimulated by normal strain, and when subsequently subject to shear strain the bone is no longer able to withstand even small loads. Given that the focal area of low strain energy density caused by eccentric axial loading elevated intracortical remodeling while the disparate neutral axis (torsional loading) retained the status quo, we conclude that high gradients of strain are somehow responsible for stimulating the lesion.

#### **Military Implications**

Extrapolating these data to military training regimens, it appears that neither high amplitude strains nor material fatigue are the cause of the stress fracture lesion. Redundant loading activities (e.g., long marches), regardless of intensity (i.e., walking vs. running), will accelerate this condition. Regimens which diversify activity (e.g. obstacle course) will most likely minimize the appearance of intracortical activity. Combining the two practices (obstacle and long marches) may well exacerbate the condition. Unfortunately, even though these rather controversial conclusions are strongly supported by the data generated by these studies, because of the contract's termination no further action can be taken to finally identify the causative agent for the stress fracture lesion.



### Introduction

Without challenge, stress fractures are the military's principal medical concern during recruit training. Despite the crippling physical, economic, and morale burden caused by this condition, the pathophysiology of the lesion remains poorly understood. The most accepted etiology is that the stress fracture lesion is the result of fatigue induced microdamage. In other words, the repetitive activity inherent in training will generate small fractures in the bony material at those sites which are subject to the greatest strain (Chamay & Tschantz 1972; Burr et al. 1985; Daffner 1978; Leveton 1946; Markey 1987; Matheson et al. 1987; Nussbaum et al. 1988). These small cracks would in turn accumulate until the risk of fracture becomes reality, not unlike the breaking of a paperclip (Frost 1960). Ironically, as dear as this etiology is held, there is essentially no evidence that repetitive activity *in vivo* will cause this material breakdown, even in the most active populations (Rubin et al 1985). Considering that evidence to support a microdamage theory is so elusive, we have formulated an alternative SFx hypothesis which directly countermands the "fatigue failure" of the bone. Importantly, the etiology arising from this new hypothesis more soundly explains the SFx pathology observed within human biopsies (elevated intracortical porosis, absence of material damage within the cortex). Further, this work has identified specific components within the loading regimen which exacerbate the intracortical pathology.

The experiments performed in our first contract (DAMD 17-86-C-6088) demonstrated that the most extensive bony defects associated with excessive cyclic loading are not those resulting from an actual material "fracture" across the cortex. Instead, the large area of rarefaction, in both the equine and avian model of stress fractures, were the result of a focal area of high bony turnover, dominated by incompletely infilled haversian systems and resulting in intracortical porosities (Jones et al. 1989; Rubin et al. 1986). Rest, regarded as a conservative treatment of this condition, may permit the intracortical remodeling to desist. However, continued abuse may indeed result in material damage (and ultimate failure), but only after the remodeling has compromised the integrity of the tissue (see C. Rubin, Final Report of Army Contract DAMD 17-90-7-0054, March 1990).

As surprisingly, the location of this lesion, relative to the distribution of strain generated across the bone during functional loading, correlates best with those areas of the cortex exposed to the *lowest* strain magnitudes, not those sites subjected to the highest deformations (Rubin et al. 1986, 1989a,b). Based on these preliminary results, we have concluded that the bony remodeling *precedes* the material breakdown, and that the turnover is an "adaptive" response to some undetermined aspect of the loading milieu that is *not* peak strain magnitude (Rubin et al. 1987).

From this evidence, we conclude that the resorption of the cortex (and the eventual failure of the bone), is a cycle dependent, focally resorptive response stimulated within the bone "tissue," rather than a frank failure of the bone "material" due to matrix fatigue. As the response was highly specific to the area of the neutral axis, it was proposed that diversifying loads would diminish the appearance of the intracortical remodeling. Further, as the strains are least at the neutral axis, it was concluded that the response was intensity independent. The evidence supporting this conclusion is extensive, and given the cross-species similarities in the pathology, allows for a powerful extrapolation to the human condition.

These initial observations led to the construction of a new hypothesis which would evaluate the role of strain distribution, cycle number, and strain intensity to the generation of the stress fracture lesions:

*Although cycle dependent, the stress fracture lesion is not a result of accumulated fatigue microdamage, but instead is a very specific and localized remodeling response which occurs at, or near, the neutral axis of loading (the site of least strain deformation). Therefore, the greatest determinant of the SFx lesion would be repetitive cyclic activity, regardless of its intensity.*

The contract, as originally reviewed, had three sub-hypotheses and five specific aims to address this general hypothesis. Unfortunately, budgetary cutbacks in the military have precluded the full funding of this program, so that the results of the first phase only could be addressed. This phase was constructed to test the hypothesis that the SFx lesion was a product of a physical regimen which limits and focuses the neutral axis of loading to a very specific area of the cortex. This sub-hypothesis is pursued through two specific aims:

**Specific Aim 1a: Axial vs. Torsional Loading.** Will torsional loading, which does not generate a specific neutral axis, diminish the likelihood of the SFx lesion (elevated intracortical remodeling) which normally appears following repetitive axial loading?

In Specific Aim 1a, the relative remodeling response to repetitive bending strains generated by eccentric axial loading was compared to a similar regimen of torsional loading. In each case, repetitive cyclic loading of 5,000 cycles per day was applied over a four week period (total cycle number; 100,000). Four weeks was chosen to both increase the number of successful completions of protocol (as opposed to eight weeks), yet ensure that the pathology generated would be well advanced by this stage (as opposed to two weeks). Peak strain magnitudes of 1000 microstrain generated at 10,000 microstrain/second, was applied within each experimental group. Because of the high cyclic numbers required in this and the following protocols, we correctly anticipated a high (40-50%) incidence of pin loosening prior to the completion of the 4 week experimental period. In each of these cases, the animals were euthanized immediately. Seven animals were required for the axial condition, and eleven for the torsion condition to achieve five successful experiments per protocol.

**Specific Aim 1b: Specific vs. Diverse Neutral Axis.** Will a loading regimen which focuses a neutral axis (axial), when combined with a loading condition with a disparate axis (torsion) diminish the appearance of the SFx lesion?

In Specific Aim 1b, the relative remodeling response to repetitive axial loading, followed by torsional loading, was compared to the remodeling response engendered by axial or torsional loading alone as observed in Specific Aim 1a. The ulna preparation was subjected to 2,500 cycles per day of axial loading, followed by 2500 cycles per day of torsional loading each day over a four week period. The total number of axial plus torsion loading cycles was therefore identical to that applied in each exclusive loading condition of Specific Aim 1a. Peak strain magnitudes of 1000 microstrain, at a rate generating 10,000 microstrain per second, were applied to this experimental group.

### Military Significance

The goal of this research program was to improve our understanding of the mechanopathophysiology of the stress fracture lesion. Only by identifying the causative agent of the lesion can the training regimen be effectively altered to suppress those parameters of the functional milieu which exacerbate the condition (Gardner et al. 1988). During peacetime, stress fractures are one of the most frequent physical training injuries observed in the U.S. military population (Jones et al. 1989; Schmidt et al. 1982), evident in up to six percent of male (Scully & Besterman 1982), and twenty percent of female basic trainees (Brudvig et al. 1983; Protzman & Griffis 1977; Friedl et al. 1992). In addition, older recruits (over 21) are more susceptible to this injury than younger trainees (Gardner et al. 1988), yet a history of athletic activity will not necessarily suppress the lesion (Swissa et al. 1989). This injury is not unique to the Armed Forces of the United States (Chisin et al. 1987; Giladi et al. 1985), other countries have reported stress reaction incidence in recruits as high as thirty percent (Milgrom et al. 1985a,b). Catastrophically, this incidence will rise in times of war, concurrent to the accelerated induction of trainees (Swissa et al. 1989; Bernstein & Stone 1944). Consequently, this stress reaction jeopardizes not only recruit health, safety and morale, but severely compromises the military's medical and defense resources (Greaney et al. 1983). Indeed, stress fractures are the leading cause of time lost in basic training (Scully & Besterman 1982; Leichter et al. 1989). As they require at least 6-8 weeks of rest without weight bearing for adequate healing, they also represent a severe increase in the cost effectiveness of recruit training (Milgrom et al. 1985a; Jones et al. 1989).

The initial symptoms include a reluctance to bear weight on the affected appendage, and are associated with acute "point pain" on palpation (Floyd et al. 1987; Chisin et al. 1987). These symptoms, although difficult to identify radiographically, coincide with focal areas of increased Technetium uptake evident during gamma scan evaluation, reflecting accelerated bone cell activity (Milgrom et al. 1985c; Zwas et al. 1988; Goldfarb 1988; Marguiles & Altan 1984). While the stimulation of periosteal new bone formation (modeling) may make the immediate area "tender to the touch", it is certainly *not* the addition of tissue that causes a bone to fracture. Indeed, it is the elevated intracortical remodeling that puts the bone at structural risk. Ignoring the conservative treatment of rest, the stress fracture lesion can proliferate to a radiographically visible area of rarefaction (Chisin et al. 1987; Zwas et al. 1987). Continued abuse can engender bony defects such as hairline fractures (Uthoff & Jaworski 1985), or even complete structural failure (McBryde 1985). Strangely, that the pathology is in fact a response to accumulated microdamage has never been established (Harris et al. 1988; Burr et al. 1985). Indeed, that the tibia's physical properties are unchanged (if not improved) following the running of a marathon (Rubin et al. 1987a) diminishes the likelihood that physiologic levels of loading engender damage. Considering that close to 50% of total SFxs are reported following only the first week of military training (Gardner et al. 1988) the "accumulated damage" theory is compromised even further, as seven days is insufficient time to surpass even the most pessimistic projections of bone's fatigue life when subject to physiologic levels of strain (Carter et al. 1981a). Interestingly, one week is precisely the time period in which remodeling response could have mobilized osteoclastic resorption of the cortex (Bain and Rubin, 1990). As the osteoid which is being laid down to replace the resorbed bone has not yet mineralized, it is not possible that this new tissue could yet supplement the bone's diminished strength.

Attempts to reduce the incidence of the stress fracture lesion have achieved only a limited degree of success (Bensel 1986; Scully & Besterman 1982; Duker 1982). This is largely due to our poor understanding of the mechanical factors (stress, strain, strain rate, strain distribution, number of strain repetitions) which are actually responsible for causing the pathology within the bone tissue (Rubin & Hausman 1988; Brand & Rubin 1988, Brown et al. 1990). The objective of the series of experiments reported here was to determine to what extent repetitive cyclic loading, applied with magnitude, manner, and duration parameters relevant to basic training, may be "perceived" by the bone as a resorptive stimulus, the precursor to the stress fracture lesion. The impact of an improved understanding of the stress fracture pathogenesis on the health and well being of the recruit cannot be underestimated.

### Overview of Previous Results

The objective of our first contract with the Army, DAMD-A-86-C-6088, was to determine the extent to which excessive repetitive loading at physiologic magnitudes would produce deleterious remodeling within limb bones, ultimately resulting in structural damage. The study was divided into three parts; a) the changes which occur in bone strain distribution concurrent to metabolic fatigue, b) the skeletal remodeling response to excessive repetitive loading, and c) the correlation of the animal pathology with that observed in the human.

In the first objective, the quantification of the strain milieu of the horse cannon bone, has allowed us to model the mechanical environment to which bones are subjected during extreme functional activity. The cannon bone model is essentially the only other site, other than those in the human skeleton, in which the stress fracture will occur naturally (Gray & Rubin 1987; Rubin et al. 1989a; Nunamaker et al. 1987; Koblik et al. 1986). By determining the strain milieu to which the cannon bone is naturally exposed, we were able to correlate the site of the pathology with the types and magnitudes of strain to which this area of the bone is subjected (Rubin et al. 1989b). In addition, we were able to determine if this manner of loading was altered following metabolic fatigue (Rubin et al. 1989c).

With the second objective, the use of the externally loadable avian wing preparation has proven very successful in providing us the initial understanding of the etiology of the "stress fracture" condition. Specifically, this animal model has provided unique (*albeit* controversial) experimental information as to the mechanopathogenesis of the lesion (Jones et al. 1989; Rubin et al. 1984, 1986, Harris et al. 1988). Further investigation, using this *in vivo* model, has begun to define those components of the functional loading environment which are most potent in their capacity to accelerate intracortical remodeling and therefore the "stress reaction" pathology (Rubin et al. 1984, 1985, 1989b,c). This, in turn, could identify specific exercise regimes which should be amended or avoided in the training program in order to diminish or eradicate this injury.

Finally, the pathology generated in both the equine and avian models were qualitatively compared to that observed in human biopsy material from the AFIP (Rubin et al. 1986; Harris et al. 1988; Jones et al. 1989). By defining the cross-species similarities in the

skeletal tissue response to excessive cyclic loading, a powerful extrapolation to the pathomechanics responsible for the human condition are possible.

**a) *Changes in the distribution of strain concurrent to metabolic fatigue***

The primary objective of this series of experiments was to establish a protocol capable of monitoring changes in the metabolic level of fatigue incurred in the exercising horse, and correlate these changes with any simultaneous alterations in the distribution of strain across the third metacarpal (MCIII). Our initial hypothesis for the appearance of the lesion was that metabolic fatigue concurrent to extreme levels of exertion would result in the recruitment of new combinations of muscular activity thereby altering the "normal" distribution of strain across the bone. This "new" distribution would in turn stimulate an adaptive remodeling response, and, secondary to the intracortical remodeling, cause the extracellular matrix to fail. However, although achieving numerous indices of metabolic fatigue (i.e. based on VO<sub>2</sub>, respiratory quotient, blood lactate), no fatigue-induced shift in the manner of loading at the level of the bone could be observed.

Following acclimation training on a motorized treadmill, eight horses were surgically instrumented, under a general halothane anesthesia and under aseptic conditions, with three rosette bone bonded strain gages. Through medial and cranio-lateral incisions, three, three-element rosette strain gages were attached to the surface of the medial, cranial, and lateral aspects of the diaphyseal midshaft of the cannon bone (MCIII). This was performed by removing 1 cm<sup>2</sup> of periosteum, and degreasing the bone with anhydrous ether. The gages were then attached using 2-isobutyl cyanocrylate, and strain relief flanges screwed to the bone, approximately 2 cm from the gage site, to minimize tension on the lead wires. All wounds were then sutured closed, and the limb bandaged (Rubin et al. 1989b,c). Gage locations and geometric properties of the cannon bone were determined using radiographs and computer aided tomography (CAT scanning) respectively. As the trauma to the animal was minimal, a full exercise protocol was possible the following day.

Three three-element rosette gages, generating nine channels of strain data from the bone, give direct indications of the magnitude of strain generated on the bone's surface as a result of activity. The "raw" strain from each gage is analyzed to give normal and shear strains from the three gage locations, and allows for the calculation of distributions of normal strain, shear strain, and strain energy density across the bone. We have monitored these distributions such that any changes concurrent to the onset of metabolic fatigue would be observed.

Prior to this work, the analysis of bone strain has been limited, as they have required simplifying assumptions regarding the inertial loading environment of the bone which may result in potentially incomplete, underestimated, or even erroneous descriptions of the bone's mechanical environment. Here, by attaching three triple-rosette strain gages to the surface of a bone across the same transverse plane and using a combined beam theory and finite element model analysis, *a priori* inertial loading assumptions are not required to define the complete strain environment of the bone's cross section. Essentially, this analysis provides a detailed mechanical profile of the bone through a cortical cross section, at any point in the stride and through a series of strides at any given speed.

For purposes of this study, a series of twenty strides were interpolated from each steady-state condition to create a single representative average stride. Longitudinal normal and shear strains were calculated at each periosteal rosette site with respect to a local coordinate system aligned with its z-axis parallel to the long axis of the bone. Normal strain distributions ( $\epsilon_{zz}$ ) were determined by modeling the metacarpal shaft as a prismatic beam of irregular cross section subjected to axial loading and bending moments. Shear strains acting upon the midshaft cross section ( $\epsilon_{zx}\epsilon_{zy}$ ) were resolved by modeling the third metacarpal as a prismatic cantilever subjected to end shearing forces and a torsional moment. In this analysis, equine cortical bone was assumed to be linearly isotropic with a Young's modulus of 18 GPa and Poisson's ratio of 0.3, while irregular cross-sectional geometry was approximated by a finite element mesh consisting of 100 quadrilateral elements. Using finite element, shear strains were determined at each element center. Initial loading conditions consisted of an arbitrary torsional moment and end shearing forces in the x and y directions, which were subsequently scaled such that the numerically determined strains at elements corresponding to the strain gage sites matched the strains measured *in vivo*. As with normal and shear strains, the distribution of strain energy density (SED) through the cross section was determined throughout the gait cycle.

Strain energy density represent the sum of all strains acting at a site; in essence, a measure of those areas undergoing the greatest level of "work". This is important as high levels of shear may correspond to low levels of normal strain, and vice versa. This calculation has allowed us to identify those areas that see the greatest (and least) strain distortions during activity. If the stress fracture lesion were generated by high levels of microdamage, they would predominate in the site of the cortex subjected to either highest normal strain, shear strain, or strain energy density.

As examples of these calculations, we can show the distribution of normal strain generated during a trot at 6.5 m/s. At the peak strain magnitude of the stance phase, the normal strain distribution shows a strain magnitude of 2459 microstrain on the medial cortex, with the neutral axis of strain running through the lateral cortex (Gross et. al., 1992). Given only this plot, it is possible only to consider the strains represented by these normal strains, i.e., strains at the neutral axis are zero. However, this calculation is not sensitive to the deformation caused by shear. With the calculation allowed by the three rosette gages, a shear distribution can be established. This demonstrates, at each location within the cortex, the levels of shear that the bone is subjected to. In this case, shear strains of 1889 microstrain are attained, the location of which are well removed from the site of peak normal strains. As bones do not normally fail under compressive strains, but rather to shear strains due to bending and torsion, i.e. the yield to failure in shear is approximately 40% that of compression (Hayes & Snyder 1981), and much smaller shear strains could have a very significant and deleterious effect on the structural integrity of the skeleton. Indeed, relationship of shear to longitudinal modulus becomes extremely important in considering the frank fractures which occurred in the most recent experiments.

This analysis, for the first time, allows for the complete mechanical milieu generated on the cortex to be characterized at any time period in a stride taken at a certain speed. This manner of loading, either through the stride of speed range, changes very little (Gross et. al.,

1992). What is of critical importance is that the areas of greatest normal strain, shear strain and/or strain energy density in the horse cannon bone are also the areas of the cortex that have the least remodeling activity. Indeed, the most common quadrant in which stress fracture lesion appears, the antero-lateral cortex (Koblick et al. 1986; Nunamaker et al. 1987), is the area of the cortex exposed to the least strain, be it normal, shear or strain energy density. What this extensive analysis has provided, therefore, is *not* only direct correlation between presence of the stress fracture lesion and the site of lowest normal strain, but emphasizes that the lesion also appears in the area of least shear and "total" strain. This emphasizes that the stress fracture lesion is not a product of accumulated damage or material breakdown, but is a by-product of a loading environment that sees high numbers of cyclic load reversals, with the pathology occurring at sites of the *smallest* deformations (Rubin et al. 1984, 1986, 1989a,b).

It has also been proposed that, if *metabolic* fatigue is achieved, new muscle recruitment patterns would be stimulated and result in altered bone loading patterns to which the skeleton is not attuned to resist (Rubin et al. 1989c). To determine if changes in the distribution of strain within the bone will parallel exercise induced changes of the respiratory/cardiovascular system, we monitored alterations in strain patterns concurrent to a series of metabolic indices of fatigue. To achieve this correlation, oxygen consumption, heart rate, and venous lactate concentration were obtained through respiratory gas measurements and blood samples drawn while the animal was exercising. A plateau in the oxygen consumption of an animal is an objective indicator of maximal aerobic power (MacLaren et al. 1989). The ratio of carbon dioxide production to oxygen consumption (respiratory quotient, RQ) indicates the extent to which respiration can provide the energy requirements of the animal, and values greater than 1.2 indicate a substantial reliance of anaerobic metabolism. Similarly, an abrupt increase in blood lactate levels indicates increased anaerobic activity. An RQ over 1.2, with a maximal heart rate, maximal oxygen consumption, and an abrupt increase in lactate levels are the standard clinical signs of metabolic fatigue.

A standard metabolic fatigue test regimen for horses was used, entailing one minute interval training at 4.5, 5.5, 6.5 and 9 meters/sec with the animal running on a 10% incline on a motorized treadmill. In this study, all metabolic tests were run on the animals both before and following surgery. Presurgery, heart rate reached its maximum value during the 5.5 m/s interval and oxygen consumption reached a plateau during the 6.5 m/s interval. Following 45 seconds at 9 m/s canter, RQ exceeded 1.2, max VO<sub>2</sub> had begun to decline, and lactate levels increased significantly, demonstrating that the animal had reached a definite state of metabolic fatigue. This also corresponded to an apparent loss of coordination of the animal and unwillingness to continue running on the treadmill. Following surgery, none of these metabolic limits changed significantly indicating that the surgical procedure did not diminish the animal's performance.

Presumably, if fatigued muscle groups had engendered new recruitment patterns, then a new strain distribution would result in the initiation of remodeling activity. As the first step of remodeling activity is the resorption of bone, the initiation of extensive remodeling could lead to bone failure. Comparing the distributions of normal strain, shear strain, and strain

energy density for the peak load condition of both pre- and post-fatigue conditions, only very subtle changes in the physical milieu of the bone could be identified (Rubin et. al., 1989c). This data demonstrates that there are no alterations in the manner of loading of the bone with the onset of metabolic fatigue. The work reported here does not support the hypothesis that metabolic fatigue would induce new bone loading patterns, and emphasizes that alternative etiologies be considered for the occurrence of such fractures.

What has been demonstrated from these studies, however, is that the area of the cortex which experiences the SFx pathology does not experience high levels of *any* sort of strain. It must be emphasized that this location is well below any threat of yield failure, and there are many areas of the cortex subject to much greater magnitudes of strain. Therefore, an explanation of the SFx must not depend on magnitude of strain, but by the manner in which it is loaded. In other words, the fracture, although ultimately caused by a material breakdown, is not initiated by damage but by remodeling. It would appear the lesion is secondary to a cycle dependent tissue response to the loading environment. Due to the complex ultrastructure and mechanical behavior of bone, deformation of the tissue results in a number of associated factors, including fluid pressure, fluid flow, and streaming potentials. Perhaps this low deformation area is also the site of extremely poor fluid flow or suppressed tissue perfusion, concurrently minimizing components of a streaming potential or causing poor nutritive exchange and hydration. Mechanisms aside, the correlation of low strain energy density to the stress fracture lesion would dismiss material failure *per se*, and requires other pathogeneses, such as the minimal fluid exchange which occurs in this area, to be proposed as responsible for the pathology.

In summary, these locomotor experiments have correlated the lesion to the area where both the normal strain and shear strain is low, and the resultant strain energy density is smallest, diminishing the possibility that the lesion is a result of accumulated microdamage. In addition, metabolic fatigue does not induce a new loading environment, diminishing the possibility that the remodeling observed at the lesion site was stimulated by "adaptation" to a new loading environment. Therefore, we conclude that some aspect of the specific cyclic loading environment, having essentially nothing to do with fatigue microdamage, stimulates focal and deleterious remodeling, leading to secondary structural failure.

***b) Skeletal remodeling response to excessive repetitive loading***

The primary objective of this series of experiments was to correlate the adaptive tissue pathology to the physiologically relevant magnitudes, rates, and durations of applied dynamic loading which caused it. This protocol exploits an established *in vivo* model developed to monitor the remodeling activity in bone generated by specific, controlled mechanical stimulation.

To investigate the mechanopathogenesis of stress fractures induced by high repetitions of a uniform exercise regime, we utilized the functionally isolated *in vivo* avian wing preparation previously reported (Rubin & Lanyon 1984, 1985, 1987). With this model, controlled intermittent loads from a modified Instron machine are applied to the functionally isolated ulna via transfixing pins. The loads of the servohydraulic actuator are adjusted to produce peak longitudinal normal strains at the midshaft from a range of 500 to 4000



microstrain, levels determined to be physiologic when compared to strains measured from a variety of skeletal locations during activity (Rubin & Lanyon 1982). In this protocol, the applied strain waveform was sinusoidal with a maximum loading and unloading rate of 50,000 microstrain/sec., also physiologic in magnitude. Each ulna preparation was subjected to regimes up to as many as 30,000 cycles/day, over a single period of loading, for five days/week. Loading was discontinued either when the animals showed discomfort or at 8 weeks, whichever was the sooner.

The maximum effect of an osteogenic mechanical stimulus was generated following only a very short exposure to an intermittent load regime (thirty-six load reversals), increased cyclic loading by a factor of fifty did not stimulate additional bone formation (Rubin & Lanyon 1984). The importance of the dynamic state was also demonstrated, static load regimes, applied at similar strain magnitudes, were ignored as an osteogenic stimulus, and osteoporosis was generated (Lanyon & Rubin 1985). Following these observations, the avian wing preparation was loaded for 100 cycles/day to determine the role of strain magnitude as an osteogenic stimulus (Rubin & Lanyon 1987). The amount of new bone formed was directly proportional to the magnitude of the engendered strain. When loaded for 100 cycles per day, this dose-response phenomenon produced essentially no new bone at 1,000 microstrain, yet was sufficient to inhibit the osteoporotic response. A 15-23% increase in bone cross-sectional area was stimulated at 2,000 microstrain, and a 28-42% increase in new bone at 3,000 microstrain. These experiments emphasize that the osteogenic stimulus can be triggered by very few cycles of a dynamic load regime, and for the stimulus to be adaptive it *does not need to be* hyperphysiologic in amplitude.

In the series subjected to excessive repetitive cyclic loading (30,000 cycle/day), a similar increase in bone cross-sectional area was elicited, suggesting that the cells responsible for new bone formation had been stimulated to work at their peak capacity by exposure to the first "few" loading repetitions. However, while microradiographs of the ulna midshaft from the 100 cycles/day animals demonstrated the degree of intracortical remodeling series to be very low, in the 30,000 cycles/day series the intracortical remodeling was extensive (Rubin et al. 1984, 1986; Jones et al. 1989). This would suggest that *two separate and distinct mechanisms exist*; one responsible for bone modeling (new bone formation), and one for bone remodeling (intracortical tunneling). Interestingly, the large structural defects which were apparent in the bone cortices were *not* cracks or microdamage, but rather the area of rarefaction consisted of resorption spaces and expansion of vascular channels. These studies represent *in vivo* remodeling data in response to cyclic loading of up to 1.5 million cycles without failure of the preparation. Even under these extreme conditions, there was no sign of extracellular tissue damage whatsoever, only an increase in focal intracortical turnover. These spaces, combined with the exuberant periosteal new bone formation with which they were associated, presented a remarkably similar appearance to the stress fracture pathology observed in the human material (Harris et al. 1988).

To correlate the pathology to the applied mechanical milieu, strain gage studies (similar to those described above) were performed to establish the specific distribution of applied strains. As was the case with the equine pathology, the region of the cortex which contained

the most consistent, extensive intracortical remodeling was not that subjected to the greatest strain (the area of the cortex most likely to accumulate microdamage), but rather was located about the bone's neutral axis, the area of the cortex subjected to the *smallest* normal strains.

Using the rigorous mechanical analysis developed for the horse metacarpal study, it was also possible to calculate not only the normal strain distribution, but the shear strain distribution and strain energy density. This analysis emphasizes that the location of the stress fracture lesion in the bird ulna appears within the area of the cortex with the smallest strain deformation, not the areas subject to high magnitudes. As in the horse study, the stress fracture lesion appears at a site of minimal shear and strain energy density, emphasizing the observation that the response was triggered by some aspect other than material microdamage (Rubin et al. 1989).

### c) *Correlation of animal models to human pathology*

The primary objective of this series of experiments was to correlate the pathology observed in the human condition to that engendered in the animal models, thereby providing a basis of extrapolation from one species to another. During the period of the first contract a large collection of human "stress fracture" or "stress reaction" material was reviewed at the Armed Forces Institute of Pathology in Bethesda, Md. (Harris et al. 1988). Of one hundred and twenty-one cases thus coded, sixty-one had sufficient historical, radiographic, and histologic materials to permit fitting into a time oriented sequence. Unfortunately, the functional strain levels to which these cases were exposed remains a matter of conjecture since exact exercise regimes were seldom available from the historic material.

In these clinical cases, frank stress fractures were distinctly in the minority. Where they occurred, the changes seen radiographically and histologically were compatible with the duration of fracture repair delineated by the case report. Of great relevance to this experimental protocol were the cases of "stress reaction" that were biopsied prior to any evidence of gross structural failure. In these cases, the cortical remodelling and periosteal and endosteal new bone formation was *essentially identical* to the histologic changes observed in the avian model, particularly those avian subjects whose loading history was of several weeks duration. (The histologic findings of the human biopsy data, and their correlation to the animal studies, is reviewed in depth in Jones et al., 1989). While there was marked deposition of periosteal new bone formation (perhaps accounting for the increase in Technetium uptake seen in other studies; Giladi et al. 1985; Milgrom et al. 1985b), there was virtually an absence of extracellular matrix microdamage. Instead, focal areas of intracortical remodeling was widely apparent, which appeared to coalesce into a trans-cortical lesion. Indeed, it would appear that the tissue was adapting in response to a "non-destructive" stimulus, a reparative "reaction" to accumulated damage was absent.

Given the strong similarities between the pathology observed in the clinical presentation of training-induced stress fractures and that demonstrated in both the equine and turkey models, an extrapolation from the quantified mechanical milieu of the animal studies to that unquantified situation in the human seems warranted. Indeed, we would conclude, based on the integration of these three studies, that the lesion in the human is a result of an aberrant remodeling stimulus, driven not by a pressure to repair extracellular matrix damage, but somehow influenced by the cyclic nature of the signal which stimulates

resorptive remodeling activity. Further, it is the remodeling, or intracortical, response that puts the bone structure at risk. A modeling response, or the *addition* of new bone, does not necessarily harm the skeleton and more probably is an integral part of the adaptive process which protects it.

Results from the previous contract provide strong evidence that the stress fracture lesion is a product of some factor *other* than peak strain magnitude. Indeed, it appears that the predominant sight of the lesion occurs in an area adjacent to the neutral axis of loading, a site of extremely low strains. From these data, we hypothesized that the stress fracture lesion will occur as a product of redundant activity, regardless of the intensity of the load. Further, we proposed that by diversifying the applied load conditions, i.e. applying torsion rather than axial loads, the absence of a neutral axis would diminish the appearance of the lesion. Finally, it was postulated that the stress fracture lesion would be minimized, even following redundant activity, if it was followed by torsional loading. To address these issues, a series of experimental protocols were undertaken to test a new hypothesis. Before the results are discussed, specifics of the experimental design are provided.

#### Experimental Design and Methods

In this section, the overall experimental design associated with the Specific Aims 1a and 1b are described, followed by a detailed description of the methodology implemented in the quantification of the remodeling pathology. The animal model developed to study this problem (functionally isolated turkey ulna preparation) has been demonstrated as highly applicable to the mechanopathogenesis of the SFx lesion.

In Specific Aim 1a, the relative remodeling response to repetitive bending strains generated by eccentric axial loading was compared to a similar regimen of torsional loading. In each case, repetitive cyclic loading of 5,000 cycles per day was applied over a four week period (total cycle number; 100,000). Four weeks was chosen to both increase the number of successful completions of protocol (as opposed to eight weeks), yet ensure that the pathology generated will be well advanced by this stage (as opposed to two weeks). Peak strain magnitudes of 1000 microstrain at a rate to generate 10,000 microstrain/second, will be applied within each experimental group. Because of the high cyclic numbers required in this and the following protocols, we expect a high (40-50%) incidence of pin loosening prior to the completion of the 4 week experimental period. In such cases, the animals will be euthanized immediately. Therefore, to ensure at least five successful experiments per protocol, nine animals are required for both axial and torsion.

In Specific Aim 1b, the relative remodeling response to repetitive axial loading, followed by torsional loading, was compared to the remodeling response engendered by axial loading alone as observed in Specific Aim 1a. The ulna preparation was subjected to 2500 cycles per day of axial loading, followed by 2500 cycles per day of torsional loading, each day over a four week period. The total number of axial loading cycles was therefore identical to that applied in 1a. Peak strain magnitudes of 1000 microstrain, at a rate generating 10,000 microstrain per second, was applied to this experimental group. The following sections describe the *in vitro* calibration analysis necessary to define the loading conditions, and the *in vivo* protocols in which the functionally isolated turkey ulna was

subject to 5000 cycles per day of axial loading, torsional loading, or 2500 cycles each of torsion and axial.

***a) Measurement of bone strains in vivo***

The following describes the surgical procedure, as well as the data collection, for the determination of strain generated during the applied load environment (Gray & Rubin 1987; Brown et al. 1989, Rubin et al. 1989a). Anesthesia is induced through a mask by inhalation of oxygen, nitrous oxide, and halothane, and the bird is maintained on this mixture following endotracheal intubation. Three rosette strain gages are attached, at the midshaft, to the "calibration" turkey's left ulna. One gage will be attached through a ventral incision, and two gages attached via a dorso-medial incision. Exposure of the ulna surface is prepared by removing a small (50mm<sup>2</sup>) area of the bone's periosteum, drying the exposed surface with anhydrous di-ethyl ether, and then gluing the gage to the surface with isobutyl 2-cyanoacrylate monomer (Ethicon Ltd). The leads are passed subcutaneously along the humerus and emerge through the skin at a remote incision above the shoulder. The wounds are closed and sutured, the leads soldered to a 25 pin connector, and the ulnae radiographed. The nine strain gage outputs are conditioned through bridge amplifiers, filtered at 500 Hz (6 pole Butterworth) and digitized (12 bit A/D, Metrabyte DASH-16) at 5KHz using an IBM compatible computer (AST Premium 286). The ulna is then functionally isolated such that calibration of the loading apparatus may be performed. This allows for a direct correlation of applied load and strain engendered, as well as a comparison of the magnitudes and distribution of the normal strain milieu to those generated by the applied loading conditions.

During applied loading, the raw strain is downloaded to the lab's 32 bit mainframe (Dual Chapparral III), on which software has been developed to calculate principal strains at each gage location, as well as determine the distribution of longitudinal normal and shear strain across the ulna's midshaft, for each data point throughout the period of recording. This provides a complete characterization of normal and shear strain due to eccentric axial loading, bending, and torsional conditions, as well as the resultant strain energy density.

***b) Functional isolation of the ulna***

The following describes the surgical procedure performed to prep the ulna such that controlled loads can be applied. Under a general halothane analgesia/ anesthesia and aseptic conditions, the feathers from the left wing are removed (Rubin & Lanyon 1984, 1987). The animal is then placed in a "straight jacket" in which only the left wing and head protrude and the wing is scrubbed with a betaine solution. After draping, two 15mm incisions are made over the proximal and distal ends of the ulna. One centimeter of the bone at either end is exposed, and a U-shaped template is clamped to these surfaces. Using an oscillating saw against the parallel planed surfaces of the template, osteotomies are made both proximally and distally such that a 3mm wafer of bone can be removed. This creates a preparation which is completely deprived of function, but which retains the musculature about, and nutrient and nervous supplies to the diaphysis. Using the template's two predrilled holes as guides, parallel holes are drilled dorso-ventrally through the bone 7mm from the cut surfaces, and the template removed. The caps fit snugly over the ends of the bone and when aligned, their two predrilled holes match the position of those just drilled in the bone. Methyl-methacrylate bone cement (Simplex P, Howmedica, Rutherford, N.J.) is mixed and

placed in each stainless steel cap (5cc in each cap). The caps are pressed into position, and stainless steel Steinman pins (100 mm long 4.7 mm diameter) are introduced through the dorsal incision, piercing the caps, bone and ventral musculature, emerging on the ventral surface of the wing. The design of the caps and pins provide an interference fit with the cortical bone at the preparations extremities. Therefore, the compressive load from the loading arms of the Instron is transferred via these pins to the caps, and distributed to the cut ends of the bone. For the torsional load conditions, as the magnitude of torque required to generate physiologic levels of strain in the ulna is extremely small, the pin:bone interface, combined with the load transfer of the cement, is sufficient to withstand the cyclic loading over the four week period without sign of pin loosening.

The anesthesia concentration is reduced, the two incisions sutured, and the wounds treated topically with nitrofurazone. The wing is covered in cotton gauze and wrapped snugly in elastoplast. The protruding ends of the pins are securely clamped together on both the dorsal and ventral surfaces of the wing with external fixators. The animal is fully awake and ambulatory approximately two hours following surgery. The dressings are changed every other day until two weeks post-op, at which time the sutures are removed. The wing is exposed for the remainder of the experiment. Each bird is maintained on prophylactic antibiotics throughout the experimental period. Fluorescent labels (tetracycline, xylenol orange, or calcein green) were administered at each one week interval such that the post-mortum sections can be examined under fluorescent light to determine the dynamic parameters of the intracortical remodeling (i.e. rates of new bone formation, number of active intracortical sites, lengths of active fronts, etc.). Following four weeks of loading, the animals are euthanized via I.V. injection of saturated barbiturate.

### *c) Dynamic loading of the isolated ulna preparation*

The following describes the instrumentation and procedures which allow for the controlled loading of instrumented and/or capped ulnae. Using a modified servo-hydraulic materials testing machine (Instron, Canton, Ma.), daily periods of the intermittent "dynamic" load regime are applied to the ulna preparation beginning two days postoperatively (Rubin & Lanyon 1985). The external fixators connecting the exposed ends of the transfixing pins are removed, and the pins in the wing are slid into one of the two pair of forks on the loading apparatus. For axial loads, the "handle" of the first fork is connected to the actuator (displacement piston), while the "tines" are attached to the Steinman pin which transfixes the distal end of the preparation. The second fork connects the proximal transfixing pin to the load cell, thus completing the circuit required for closed-loop feedback. A function generator (Wavetek, Model 75, San Diego, Ca.) provides the command signal to the servo-hydraulic actuator piston, while the error signal generated from the load cell is used as feedback to the load amplifier. By controlling the displacement of the actuator in this fashion, the resultant load to the bone is an accurate reflection of the command waveform.

For torsion, the transcutaneous pins are placed into a second set of forks, as above. The linear motion of the actuator is translated into rotation of the proximal end of the ulna via a simple linkage system. The distal end is set in the tines of the second, fixed fork, which, via a strain gage affixed to a central column, gives the error feedback signal to condition the command waveform.

A strain-related feedback signal cannot be obtained directly from the experimental bone preparations since attaching strain gauges to these bones would interfere with the remodeling process which we intend to investigate. Therefore, the relationship between axial or torsional loads applied by the actuator and the resultant strains engendered at the ulna midshaft were determined from calibration ulnae. The load:strain relationship from this calibration was used to determine the appropriate command signal for the desired mechanical regime. For this series of experiments, a simple sinusoidal function is used to generate a peak rate of strain of 10,000 microstrain/second at the bone surface. The relationship of load to strain is essentially linear in the physiologic range, and the neutral axis remains stationary through the applied axial loading.

This series of experiments assumed that the loads imposed on the calibration ulnae would elicit the same strain magnitude and distribution on the ulnae of the experimental group. We used turkeys of similar size and breeding, and assumed the bone loading geometries, within each population, to be identical. The data from calibration ulnae of adult males demonstrate that a dependable and repeatable approximation of peak compressive strain about the circumference of normal, healthy, bone can be calculated from the applied load:

$$1000 \mu\epsilon = 226 \text{ Newtons; } (\mu\epsilon \text{ is microstrain}).$$

The peak strain due to torsion is approximated by:

$$1000 \mu\epsilon \text{ (shear) corresponds to 2.3 Newton meters.}$$

The peak force output of the hydraulic system (4400 N), the maximum displacement of the actuator (25mm), and the peak velocity of the piston arm (71mm/sec), were more than sufficient to allow for these loading parameters.

The geometric properties of each serial section from the left experimental ulna are then compared to its matched serial section from its own "internal control" ulna. Changes in these geometric parameters rely on the assumption that the properties determined from the contralateral control ulna are similar to the pre-operative parameters of the experimental ulna. As the mechanical regime of the control right ulna does not appear affected by the functional isolation of the left ulna, an observation supported by the quiescent state of the control ulna's remodeling activity, this does not seem to be an invalid comparison. This observation is supported by the quiescent state of the central ulnas remodeling activity. In each case, we verified that areas of new bone seen on the microradiographs, as well as the intracortical turnover, were indeed generated during the protocol by viewing the section under u.v. light for the presence of the fluorescent labels.

#### ***d) Histology***

The following describes the methodology followed to harvest, fix, embed, and cut histologic sections from the calibration, experimental, and control ulnae. Post-mortem, the experimental and control ulnae from each bird are radiographed intact in two projections (A.P. & D.V.). Strain gaged ulnae from the calibration series are radiographed in three projections, such that each gage is parallel to the plane of the film, thus allowing clear definition of the relationship of the gage array to the long axis of the bone. Immediately following these radiographs, each bone is dissected free of soft tissue, and sequentially the midshaft cut at one cm. intervals on either side of the midshaft, using a low speed diamond

wheel saw while immersed in refrigerated 70% ETOH (Rubin & Bain 1989). This allowed the evaluation of 2 c.m. of tissue, a region in which the full mechanical milieu has been determined by finite element modeling (Brown et al. 1989). The bone specimens were then dehydrated in a graded series of increasing alcohol concentrations, embedded in methylmethacrylate plastic, and polymerized in a vacuum desiccator under nitrogen (Baron et al. 1983). Following polymerization, thin (5 & 7 micron), undecalcified sections from each block of bone were cut on a Jung Model K, sledge-type microtome, using a carbon-tungsten knife (HK-3). Sections for fluorescence microscopy were cut at 7 microns and mounted unstained. For light microscopy 5 micron thick sections were cut, and two staining techniques utilized. To identify and measure osteoblast and osteoclast numbers, their location, and surface extent, the sections were stained with toluidine blue. Mineralized bone and osteoid measurements were evaluated on sections stained with Goldner's trichrome.

Quantification of histomorphometric parameters were performed at 160x using bone morphometry software (BIOQUANT), for use on an IBM-AT computer. This morphometry program utilizes a digitizing pad and cursor interfaced with a light/fluorescent microscope (Nikon LABOPHOT, Epi-Fluorescent Microscope System). The scope is fitted with a camera lucida that superimposes the cursor LED on the microscope image.

To correlate the mechanical milieu with the observed site specific pathology, each section was radially subdivided into six sectors and each histomorphometric parameter evaluated within that area: To assess osteoblast function, osteoblast perimeters (active formation surface), osteoid seam widths, osteoid perimeters and areas were measured (Parfitt et al. 1987). Osteoclast activity was correlated with osteoclast perimeters (active resorption surface) and nuclei per osteoclast. These parameters were evaluated in cortical bone and cortico-endosteal bone surfaces. These measurements represent standard histomorphometric techniques, and are based primarily on methodology described in Recker's monograph on measurements of calcified tissue (1983).

Dynamic rates associated with bone formation were interpreted from sections mounted unstained for fluorescence microscopy. Periosteal bone apposition and bone formation rates (Miller et al. 1986), osteon appositional rate, and percentages of labeled and unlabeled osteons will be measured. To evaluate osteon appositional rates, the distance between 2 adjacent labels at 4 equidistant points around each osteon's circumference were measured for the active osteons observed in each sector. The mean distance between the double label, divided by the number of days in the interlabeling period, equals the osteon appositional rate and reflects osteoblast activity.

#### *e) Microradiography*

The following describes how physical and sectional property data of the remodeling bone were attained. Following the thin sectioning, two 100 micron thick undecalcified sections were harvested from the face of the identical blocks, using the Microslice II diamond edged annular materials saw (Cambridge Instruments). Therefore, this protocol yields both thick and thin sections for adjacent areas of the bone, to identify both cellular and morphologic data for the "same site". Matched serial sections are taken from the contralateral control ulna, to establish the changes which have occurred over the four week

experimental period. Microradiographs for the purpose of assessing the bone's geometric properties are made from these 100 micron sections using a Faxitron microradiography unit (Hewlett-Packard) and a single emulsion industrial film (Kodak SR-5). An eighty second exposure at 26.0 KVP and 2.4 mAs provides excellent detail in enlargements up to 30x. By mounting the matched serial sections of both the experimentally prepared and the intact control ulna on the same microradiograph, area comparisons are facilitated.

#### *f) Areal analysis*

The key to the analysis of the bone sections was the precise quantification of modeling (periosteal and/or endosteal formation) and remodeling (intracortical turnover and/or endosteal resorption) activity. A great deal of our development work focussed on optimizing these digital image analysis programs. Areal analyses were performed from digitally scanned images of the midshaft cross-section of both the experimental (left) and control (right) bone using custom-written interactive computer programs. This method greatly facilitated the accurate and repeatable measurement of the bone areal properties and porosities.

Microradiographs of the bone cross sections were photographically enlarged to approximately 8x magnification to enhance the fine structure of any newly formed bone or porosities. These black and white photographs were then digitally scanned using a high-resolution flatbed scanner connected to a NeXTstation microcomputer. Images were scanned as 8-bit (256 shade) grayscale images at a resolution of 200 dpi (fig. 1a). This procedure resulted in a final resolution of approximately  $40 \mu\text{m} \times 40 \mu\text{m}$  ( or  $0.0016 \text{ mm}^2$ ) per pixel. The images were then transferred via direct ethernet connection to an IBM RS/6000 graphics workstation for processing.

All image analysis programs were custom written using the PV-WAVE visual data analysis software package (Precision Visuals, Boulder CO). Programs were written to analyze both the areal property changes of the whole bone sections as well as the changes in number, shape, size, and orientation of porosities within the cortex. To increase the repeatability of the measurements, images were thresholded at a level equal to the half-power of the maximum intensity (i.e.,  $\sqrt{2/2} \times 255 = 180$ ) to identify areas where bone was present (fig 1b).

The centroid of the bone was determined from this image using a pixel summation technique adapted to the standard method used for calculating centroids of composite areas. The coordinates of the centroid,  $c_x$  and  $c_y$ , are given by:

$$c_x = \frac{\sum A_i x_i}{\sum A_i} \quad c_y = \frac{\sum A_i y_i}{\sum A_i} ,$$

For an image consisting of a composite of pixels,  $A_i$  is the area represented by the  $i$ th pixel,  $\sum A_i$  is the total cross-sectional area, and  $x_i, y_i$  are the centroid of each individual pixel.



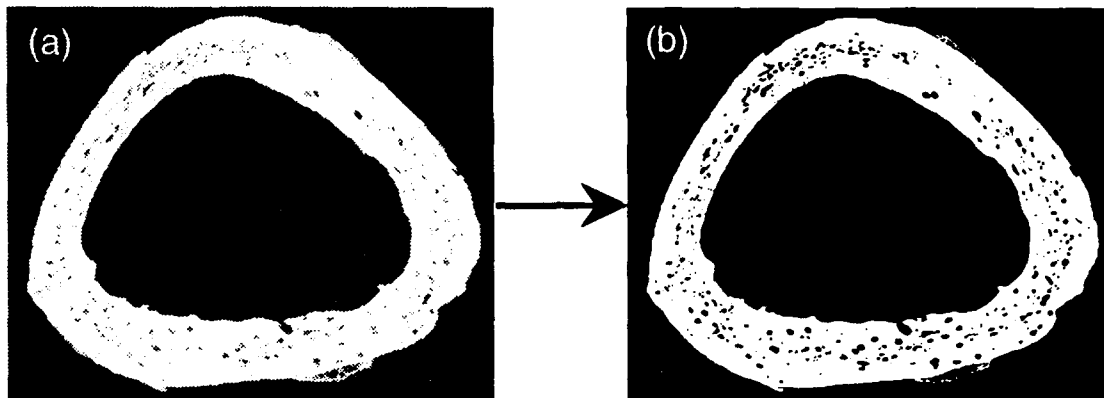


Figure 1: (a) 8-bit, 256 shade, digitally scanned image of a microradiograph is then converted to a binary image (b) used for automated and interactive analyses.

Site-specific changes in these parameters were examined by dividing the bone cross-section into six equiangular (60 degree) sectors which were analyzed separately (fig. 2). These sectors were defined based on anatomical landmarks on the ulna, with the angles converging on the centroid.

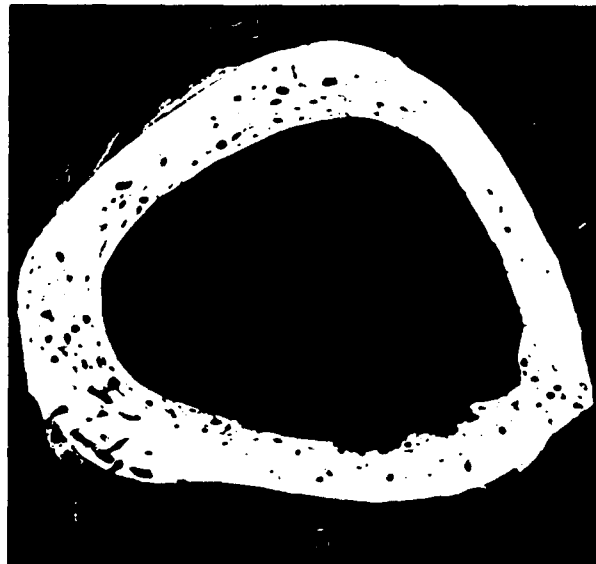


Figure 2: From the centroid of the bone, rays were projected to the endosteal surface to define the six equiangular sectors for site-specific areal and porosity analyses. When correlated to the distributions of strain (see below), sector 4 is the slice where both normal strain and strain energy density is lowest.

The areal properties of each of the six sectors of the bone were determined by digitally separating the total bone, total pore space, endosteal envelope and periosteal envelope of the cross-section (fig. 3). This analysis was performed using an interactive graphics routine used to digitally "fill" the endosteal space of the image starting at the centroid of the ulna. Similarly, the periosteal space was identified as the area outside of the ulna. At this point, it was possible to accurately distinguish each of these four regions by digitally subtracting the other three regions from the original image. A pixel summation routine was used to measure the total area encompassed by each region at a resolution of 0.0016 mm<sup>2</sup>.

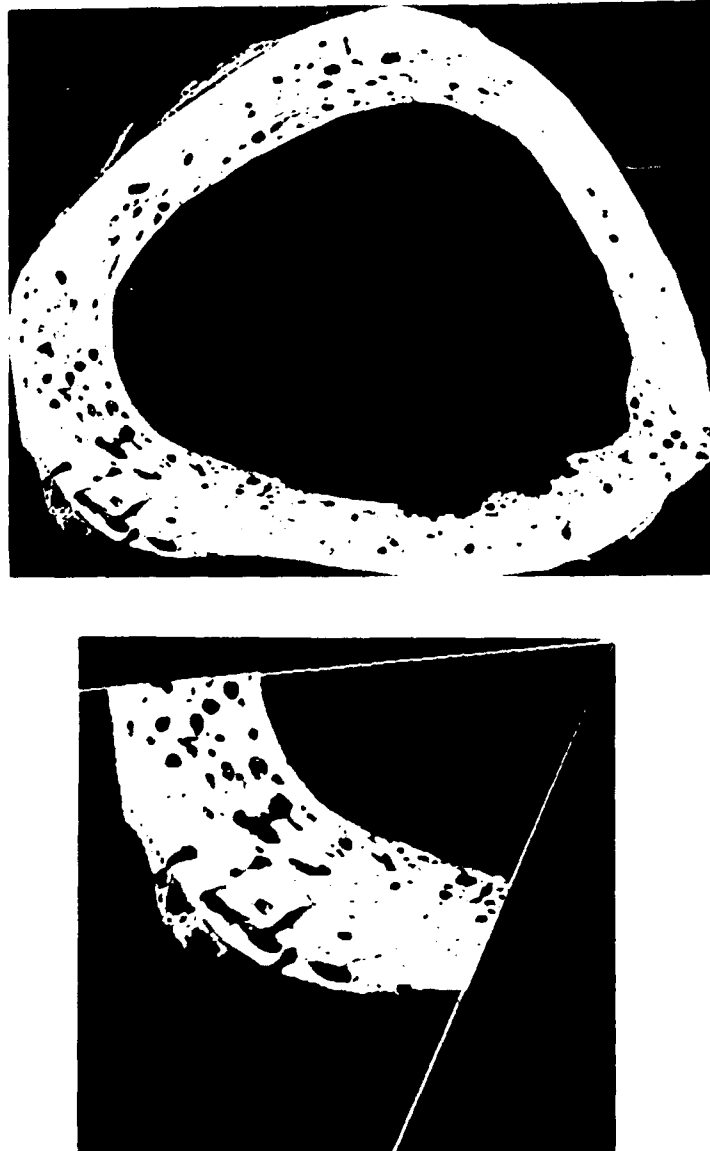


Figure 3: Digital image analysis techniques were used to separate the bone (white), pore space (black), endosteal space (red), and periosteal space (blue) in the whole bone cross-section (top), as well as in each of the six equiangular (60°) sectors (bottom) as divided in fig. 2. Sector 4 is from a combined axial/torsion ulna.

Morphometric measurements on individual porosities were performed on each of the six sectors of the image the using an interactive analysis program. For each sector, each porosity was identified and marked by an operator. The program then calculated the major axis, minor axis, and shape ratio of the porosity using a vector-tracing method from the centroid of the porosity. The orientation of the major axis of the porosity was also calculated relative to a vector between the centroid of the entire bone and the centroid of the porosity (fig. 4). In combination with the results of the areal analysis, this procedure was used to calculate the average pore size in each section.

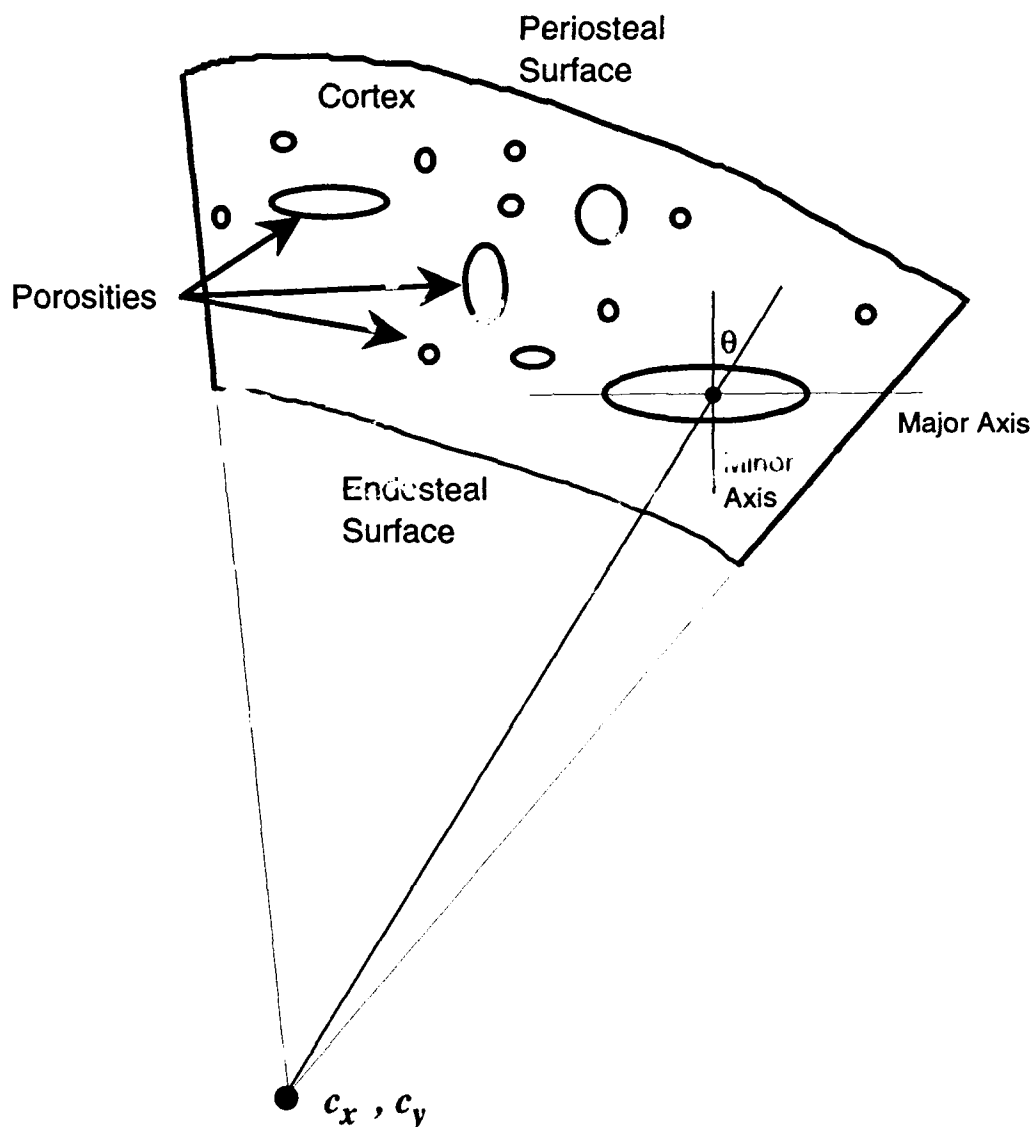


Figure 4: In each of the six sectors, an interactive computer program was used to calculate the number, major and minor axes, shape ratio (major axis / minor axis), and orientation angle ( $\theta$ ) relative to the bone centroid of all porosities.

### Final Results of Current Contract

A well controlled animal model's adaptive response to accurately known loading conditions is the ideal standard against which to evaluate plausible mechanical factors responsible for elevated remodeling. The functionally isolated avian ulna is particularly well suited for this purpose. Combined with the ideally controlled nature of the *in vivo* loading experiments, a finite element model (FEM) of the functionally isolated ulna offers the opportunity to obtain full-field strain calculations in the search for mechanical objectives, particularly when the strains are bone-specific. That is, modeling individual bones having unique geometric properties, well-characterized loading conditions, and known remodeling responses may provide more definitive answers identifying the causative agent in the stress fracture pathology. With this framework, we developed and experimentally validated a three-dimensional finite element model of the functionally isolated turkey ulna. Stresses and strains were computed for physiologic loading and for two altered (but known) loading states used in the *in vivo* studies of stress fracture etiology. We mapped the distributions of the mechanical parameter differences between the physiologic loading state and the altered loading states. We subsequently compared these mappings with observed periosteal modeling and intracortical remodeling patterns, to determine which candidate parameter - if any - could predict the distribution of the initial stress fracture response, and identify the causative factor of the focal intracortical lysis.

#### a) Defining the applied strain state of the turkey ulna model.

Determination of the experimental strain state: The left ulna of four 20 kg adult male turkeys were osteotomized, capped, and pinned following the same surgical procedure as that reported previously for *in vivo* functionally isolated ulnae (Rubin and Lanyon, 1984). Since the activities of these birds had been unrestricted, we assumed that these ulnae were in a state of remodeling equilibrium under normal physiologic usage. The animals were sacrificed and the isolated ulna preparation dissected from the wing. Rosette foil strain gages were attached periosteally at three stations around the mid-circumference, to allow beam theory-based estimates of strain distributions within that cross-section. Previous *in vivo* rosette recordings from a similar functionally isolated preparation, made under conditions of no imposed pin loading, had revealed negligible surface strains compared to those developed in the normal physiologic activity (wing flapping) of the intact ulna (Rubin and Lanyon, 1984). Thus prepared, the specimen was affixed to a loading frame in which it could be subjected to either quasistatic longitudinal compression or torsion.

Axial loading was achieved by means of Instron-controlled uniaxial displacements transmitted via a pair of steel forks which gripped the distal transfixation pin. A similar pair of forks gripping the proximal fixation pin were rigidly attached to a stationary load cell. Nine channels of strain gage output were continuously recorded for peak cyclic longitudinal loads up to 1112 N. The *in vitro* Instron-loaded specimen was then removed from the loading apparatus, embedded in a block of clear polyester resin, and transversely sectioned serially every 5 mm along its entire length.

#### b) Formulation of the finite element model.

Photographic images of the proximal face from the central section of the *in vitro* loaded ulna were projected, and the endosteal, periosteal and intracortical surfaces were digitized. These surface coordinate data (about 300 points per section for each of 21 sections) were

then input to a special purpose finite element pre-processor algorithm. The processor automatically computed nodal coordinates and element connectivities for a three-dimensional zoning scheme, based on layers of two 'concentric' rings per section, with 20 equiangular brick elements per ring. The global mesh configuration was comprised of 720 tri-linear displacement 8 node isoparametric elements, and had 3420 degrees of freedom. Ulnar cortical bone was modeled as a homogeneous, isotropic, linear elastic continuum with an elastic modulus of 11 GPa and a Poisson's ratio of 0.3 (work in progress). Stress and strain distributions were computed using the FEAP finite element program, running under the VMS operating system on a VAX 11/730 computer. Prior to undertaking computations for the actual ulna problem, we first documented the adequacy of the meshing scheme's spatial resolution by comparing computed vs. analytical stresses and flexures for a similarly zoned thick walled cylindrical cantilever beam problem.

Differing procedures were used to arrive at two distinct sets of ulna finite element boundary conditions, corresponding to the three loading states of interest (Instron axial and torsional loading of the functionally isolated ulna, vs. normal physiological wingflap loading of the intact ulna). For the Instron case, both the mid-section periosteal strains and the external kinetic conditions (i.e. the Instron load cell output and the distal fork displacement) were accurately known. For the wingflap case, the mid-section periosteal strains were known from experimental recordings, but the external kinetic conditions (i.e. the muscle and joint contact forces) were not.

The Instron loading condition was modeled by imposing equal unit longitudinal (z-direction) displacements of the six finite element nodes lying coincident with the proximal transfixation pin, while keeping the corresponding six distal nodes constrained against z-displacement. All twelve of these pin axis nodes were constrained against motion in the x-direction and all except one (rigid body motion constraint) were permitted to displace freely in the y-direction. This set of boundary conditions corresponds to an assumption of ideally frictionless and rigid pins. To allow direct comparison of the FEM results with the strain gage recordings, the computed stresses and strains were scaled in accordance with the ratio of the resultant computed reaction forces (non-zero only for the twelve displacement-constrained pin axis nodes) to the 1112 N load cell force used *in vitro*.

To simulate physiologic loading, we adopted an iterative procedure to arrive at a set of finite element boundary conditions having computed mid-section strains consistent with the mid-section strains previously recorded at the peak of vigorous wing flapping in a gaged but otherwise intact ulna. Given the very small mid-section strains known to occur during wingflap of the functionally isolated ulnar preparation, we reasoned that wingflap loading in the intact ulna must have been dominated by the articular contact forces by means of statically equivalent axial forces and bending moments applied to the proximal and distal ends of the mesh. As with the Instron case, the finite element simulation of wingflap was driven by axial displacements imposed for a set of six proximal-end nodes lying along a single ray of the mesh. Unlike the Instron case, however, neither the proper ray orientation nor the proper distribution of nodal displacements was known *a priori*. After several trials, we found that a linear variation of imposed axial displacements for the six nodes lying on the next-to-ventral-most mesh ray resulted in a computed mid-section neutral axis very

nearly coincident with that inferred from the strain magnitudes. The corresponding resultant force was an axially directed loading of 239 N, passing 2.19 mm eccentrically from the proximal end-section centroid.

There was good agreement between the longitudinal normal strains measured in the *in vitro* Instron-loaded ulna and the longitudinal normal strains computed at the site of the three gage stations (-3.26 vs -2.97  $\mu\epsilon/N$  at gage 1, 0.34 vs 0.41  $\mu\epsilon/N$  at gage 2, and -2.05 vs -2.25 at gage 3). The locus of the computed zero-strain isopleth was nearly coincident with the neutral axis inferred from a simple beam-theory analysis of the strain gage data. Moreover, the computed non-zero strain isopleths are similar to beam theory predictions, both in terms of their orientation (nominally parallel to the neutral axis) and in terms of their distribution (nominally uniform incremental spacing).

For the series of experiments to evaluate the remodeling response of torsion and axial loads, a sinusoidal function was used to generate a peak of 1000 $\mu\epsilon$  (microstrain) longitudinal normal strain (axial case) or 1000 $\mu\epsilon$  shear (torsional case) at rates of 10,000  $\mu\epsilon/sec$ . For axial loading conditions, the caps provided end-loading supplemented by cement and pins. In previous calibration procedures, we have demonstrated that an axial load of approximately 263 N reproducibly generates a peak longitudinal normal strains of 1000  $\mu\epsilon$  (fig. 5a, b).

In previous studies, the preparation has withstood up to 1.7 million cycles of such loading over 8 weeks without sign of pin loosening. As the torsional conditions cannot exploit the end-load transfer of the cap/pin implant, the cap design was modified (cement sleeve) to conform to and "clamp" the end of the bones during twisting. Calibration ulnae have demonstrated that 2.4 N-m will reproducibly generate a peak approximately 1000 $\mu\epsilon$  (shear). Torsional loads were simulated in the FEM to approximate the resultant stress/strain fields and the distribution of various parameters (normal shear and strain energy density) were determined (fig. 6a, b)

In summary, both the experimental and FEM, and analytic techniques have been developed specifically to conduct work outlined in Specific Aim 1a and b of the contract. The second phase of this contract was to pursue the hypothesis that the SFx lesion is a product of a physical regimen which limits and focuses the neutral axis of loading to a very specific area of the cortex and is independent of load intensity.

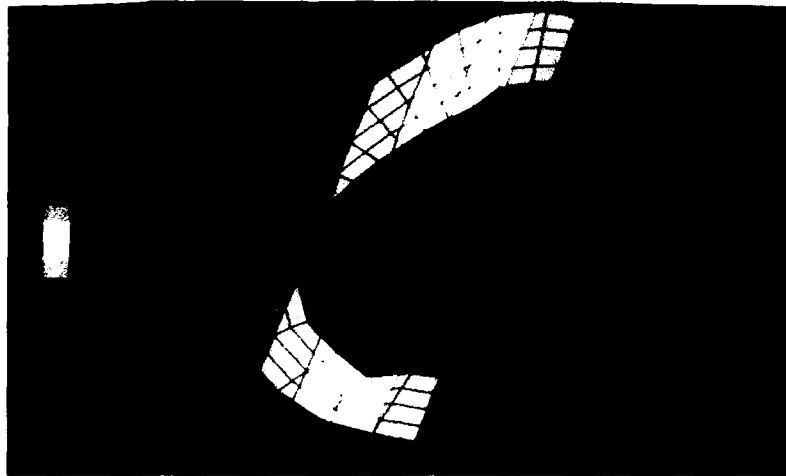


Figure 5a. Finite element solution of longitudinal normal strains induced in the ulna midshaft during axial loading. The curvature of the bone precipitated a bending environment, with peak compressive strain (blue) located in the cranial cortex (sector 6) and peak tensile strains (red) in the caudal cortex (sector 4). The neutral axis (middle yellow) transfixes the caudal and ventral cortices (corresponding to sectors 2 and 4).



Figure 5b. Strain energy density (SED) induced in the ulna midshaft during axial loading. As the strain environment was dominated by longitudinal normal strains (5a), the SED distribution was similar with sites of least strain energy (blue) corresponding to sectors 2 and 4, and the sites of greatest strain energy (red) focused within sector 6. The magnitude of strain energy varied more than 10 fold across the cross-section.

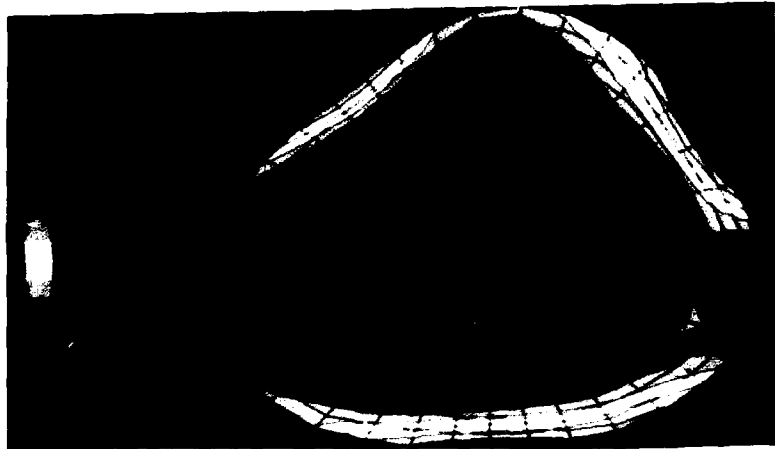


Figure 6a. Finite element solution for shear strains induced in the ulna midshaft during torsional loading. The magnitude of shear strains increases radially from the section centroid. Due to the triangular morphology of the ulna, peak shear (red) was located on the flat surfaces of the bone (corresponding to sectors 1, 3, and 5).



Figure 6b. Strain energy density (SED) in the ulna midshaft during torsional loading. Here, the strain environment was dominated by shear strains, and the SED distribution mirrors that of the shear distribution. The strain energy was more evenly distributed than during axial loading, with sites of greatest (red) and least (blue) SED demonstrating only a 4 fold difference.



**c. Differential response of bone to axial and torsional loading.**

The functionally isolated ulna model was used to study the differential remodeling response of bone to axial loading, torsional loading, axial plus torsional loading, and disuse. Four experimental and one control group were constructed with the goal of having five animals in each group complete the four week experimental protocol. The groups were as follows:

i) **Axial:** an eccentric axial load was applied to the preparation to induce strain due to bending. Loads were such to cause a peak normal strain of 1000 microstrain. Animals were loaded for 5000 cycles per day, five days per week, for a total of four weeks. Total number of cycles was 100,000. Five animals completed the protocol.

ii) **Torsion:** a torsional load was applied to the preparation to induce a peak shear strain of 1000 microstrain. Cycle and duration criteria were identical to that described in the axial group. Five animals completed the protocol.

iii) **Axial plus Torsion:** 2500 cycles per day of axial loading, sufficient to cause a peak normal strain of 1000 microstrain, was followed by 2500 cycles per day of torsional loading, inducing a peak shear strain of 1000 microstrain. Three animals completed the protocol.

iv) **Disuse:** the ulnae of five animals were isolated and left unloaded for a four week period. Five animals completed the protocol.

v) **Control:** to ensure that the remodeling observed in the functionally isolated ulna preps was indeed the product of the applied loading regimen, the contralateral ulna from each animal was used as an intraanimal control. In each case, the right ulna was left surgically undisturbed, and the areal assays performed on these "control" ulnae were then compared to the data collected from their own experimental ulna.

The areal analysis reported here focuses on three criteria; number of porotic events in the cortex, area of porosis in the cortex (in  $\text{mm}^2$ ), and change in total area (in %) as compared to the animal's intact contralateral control bone. Quantification of the remodeling change resulting from the loading regimens showed distinct responses in each case, axial, torsion, axial plus torsion, and disuse (table 1).

As a baseline, the control ulnae from these animals had a mean of 36.1 poroses per cross-section ( $\pm$ s.e.m. 18.1), with an area of bone lost by these events of  $0.202 \text{ mm}^2$  ( $\pm 0.110$ ). Therefore, the average size of a porotic event was  $0.0056 \text{ mm}^2$  (fig. 7).

In the axial group, both number of poroses ( $246 \pm 40.5$ ) and area lost by porosis ( $1.39 \text{ mm}^2 \pm 0.251$ ) was elevated substantially (7x) over that measured in the controls (fig. 8). Interestingly, the average area of a pore was  $0.0056 \text{ mm}^2$ , identical to that of control. The sector of the bone most affected by the intracortical turnover was that which was subject to the *least* normal strain and strain energy density. Total increase in area over control was  $6\% \pm 9\%$ .



Figure 7. Microradiograph of a bone cross-section harvested from an intact control bone. Note the solid cortex with relatively few porotic events.



Figure 8. Microradiograph of an ulna midshaft following four weeks of loading sufficient to cause peak longitudinal strain of 1000 microstrain. As compared to its contralateral control bone (see fig. 7), the intracortical porosis is elevated. Importantly, although the number of events has increased by 680%, the size of the porotic event has remained the same.

In the group subject to torsion, both the modeling and remodeling response essentially vanished (fig. 9). Neither the number of porosities ( $67 \pm 22$ ) nor the area lost to porosis ( $0.352\text{mm}^2 \pm 0.114$ ) was significantly different than control. The average pore size was  $0.0052\text{mm}^2$ , similar in size to control. There was no increase in bone area ( $1\% \pm 2\%$ ).

The combined axial/torsion loading proved extremely difficult to complete. Even though nine animals were committed to this group, only three completed the entire four week protocol. Indeed, the combined loading caused greenstick fractures in five animals (fig.10). These failures occurred only in this loading program. The only time such fractures have ever occurred, in over 700 loading procedures using this model, have been in this loading combination. This includes animals loaded for up to sixteen weeks and subject to over two million cycles of load three times in magnitude to that used here. Following the

fifth failure this protocol was abandoned. Of the three that completed the regimen, both the porotic number ( $298 \pm 83$ ) and area of porosis ( $3.35\text{mm}^2 \pm 0.71$ ) was significantly increased over control and torsion. Average pore size ( $0.011\text{ mm}^2$ ) was also increased over axial, control or torsion (fig. 11).

Finally, to determine if these intracortical changes were in response to the absence of a mechanical signal, we performed the isolation surgery and left the ulnae untreated for a four week period. Interestingly, although the pore number did not increase ( $58.6 \pm 22.3$ ), the area lost to porosis elevated significantly over control ( $1.05 \pm 0.35$ ). The average pore size, therefore, increased substantially to  $0.018\text{ mm}^2$ , three times the average pore size of control, torsion or axial loading. The animals lost total bone mass, dropping 13% ( $\pm 1.7\%$ ) of area as compared to control (fig. 12).

		total	s.e.m.
area of porosis in mm2	torsion	0.352	0.114
	axial *	1.39	0.252
	ax/tor *	3.35	0.71
	disuse *	1.05	0.35
	control	0.202	0.062
number of porosities	torsion	67	22.6
	axial *	246	40.5
	ax/tor *	298	83.4
	disuse	59	22.4
	control	36	8.5
percent difference from control	torsion	1.01	0.021
	axial	1.06	0.098
	ax/tor	1.11	0.086
	disuse *	0.876	0.019
	control	1	0
area in mm2	torsion	67.86	1.96
	axial	72.94	4.6
	ax/tor	69.32	2.1
	disuse *	46.18	1.5
	control	63.55	2.2

Table One. Means ( $\pm$ s.e.m.) of areal measurements made from the four experimental groups. Also quantified are the control bones, pooled across groups. Statistical significance was determined by a one-way analysis of variance. If the ANOVA  $p < 0.05$ , differences between loading protocols were determined by a student's Neuman Keuls test.

Areal analysis of each of the six sectors was also performed for the axial, torsion, axial plus torsion, and control bones. This was performed to determine if there was any correlation between those areas subject to high (or low) strains and elevated intracortical (pore number, area of porosis) or periosteal/endosteal (total area) activity. In each group, the highest level of modeling or remodeling activity was found in sector 4 (Table 2). Strangely, this sector was also the sector subject to the least normal strain or strain energy density. Consistently, whether porosis, pore number, or new bone formation, if activity was elevated it most likely occurred here.

		Sector of bone											
		s1	s.e.m.1	s2	s.e.m.2	s3	s.e.m.3	s4	s.e.m.4	s5	s.e.m.5	s6	s.e.m.6
area of porosis in mm2	torsion	0.024	0.013	0.017	0.009	0.071	0.024	0.139	0.076	0.069	0.031	0.037	0.012
	axial	0.128	0.05	0.154	0.06	0.172	0.02	0.457	0.11	0.229	0.06	0.227	0.05
	ax/tor	0.055	0.02	0.438	0.15	0.354	0.1	1.408	0.28	0.764	0.32	0.339	0.15
	control	0.0097	4.91	0.0085	7.6	0.04	0.02	0.087	0.05	0.036	0.02	0.021	0.01
number of porosities	torsion	1.4	1.25	4.8	3.98	11	4.11	27.4	16.05	13.4	5.72	9	4.37
	axial	31.2	10.68	34.8	11.94	39.6	3.67	66.2	18.84	34.2	11.47	40	10.73
	ax/tor	23.33	4.7	65.66	21.6	47.66	12.49	70	25.72	53	13.95	38.33	14.97
	control	1.92	0.88	3.23	1.83	6.15	3.68	18.15	9.02	8.076	4.32	7.166	2.73
percent difference from control	torsion	0.992	0.04	1.03	0.03	1.04	0.01	1.02	0.04	0.97	0.04	1.02	0.02
	axial	1.092	0.11	1.04	0.09	1.05	0.07	1.094	0.14	1.086	0.1	1.034	0.07
	ax/tor	1.09	0.08	1.11	0.06	0.99	0.05	1.21	0.13	1.2	0.15	1.08	0.07
	control	1	0.45	1	0.57	1	0.4	1	1.03	1	0.52	1	1.27
area in mm2	torsion	10.28	0.32	11.34	0.465	11	0.333	13.46	0.23	8.28	0.42	13.38	0.66
	axial	10.68	0.69	12.01	0.83	11.82	0.81	14.68	0.94	9.04	0.7	14.46	0.96
	ax/tor	10.5	0.28	12.63	0.26	10.83	0.36	13.6	0.62	9.63	0.68	13.6	0.43
	control	10.13	0.283	11.4	0.356	10.96	0.25	13.23	0.64	8.6	0.325	13.44	0.499

Table Two. Sector by sector analysis to determine statistically significant site-specific differences between the control section within a group, and within a section between groups. Sectors different from control are identified by a solid circle. Sectors within a group different from sector 4 are identified with a solid triangle. Following an ANOVA with a Neuman Keuls follow-up. Statistical significance was determined by one-way analysis of variance. If the ANOVA  $p < 0.05$ , differences between sectors was determined by a student's Neuman Keuls test.

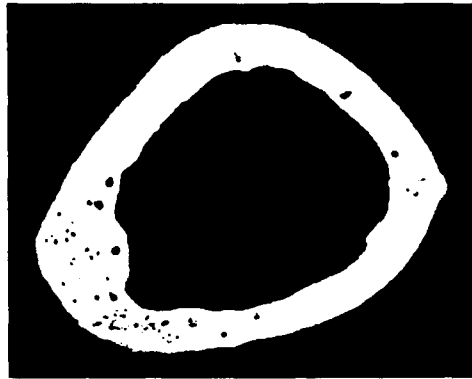


Figure 9. Microradiograph of an ulna subject to four weeks of torsional loading. This regimen, sufficient to cause 1000 microstrain in shear, caused essentially no change in either porotic event or area lost by porosities.

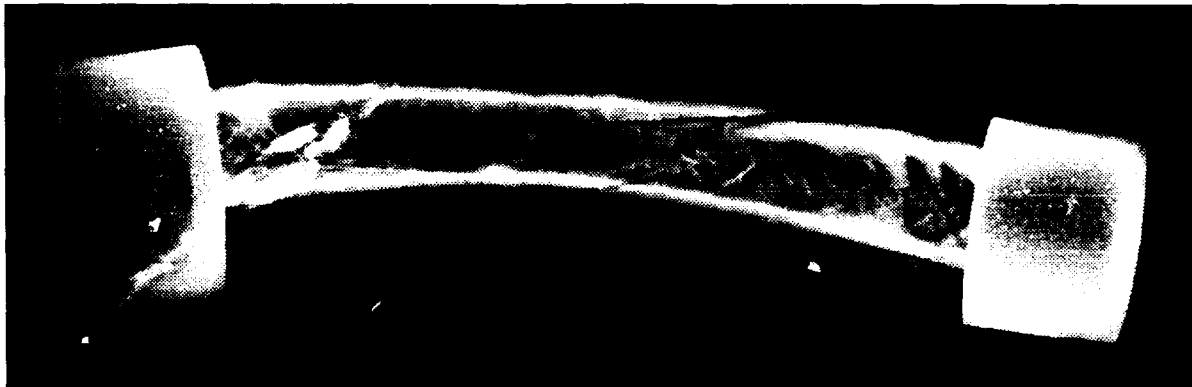


Figure 10. Radiograph of an ulna preparation which had failed due to a greenstick fracture. This combination of axial followed by torsion is the only loading condition in which a shear induced failure has ever occurred.

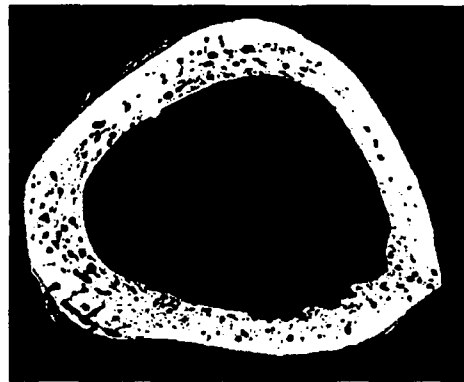


Figure 11. Microradiograph of ulna cross section following four weeks of of daily axial and torsional loading. Both the intracortical number and area of porosis has increased.

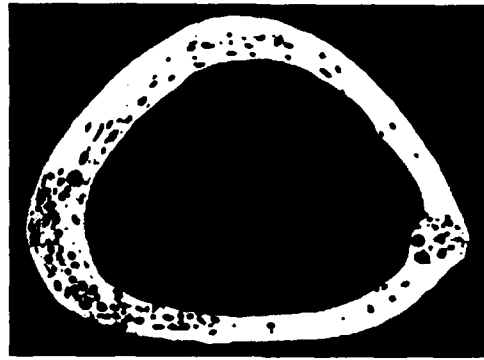


Figure 12. Microradiograph of ulna cross section following four weeks of disuse. Note the relatively large porotic events.

The data described in the above results are also presented in graph form. In Fig. 13, the mean total area of porosis are presented. In Fig. 14, the number of intracortical poroses are given. Fig. 15 shows mean total area of the midshaft for each experimental group. Sector by sector analysis is given in figures 16 & 17, showing the high level of intracortical activity in sector 4. Figures 18 & 19 show the differential response of sector 4 to the applied regimes.

### Area of intracortical porosities

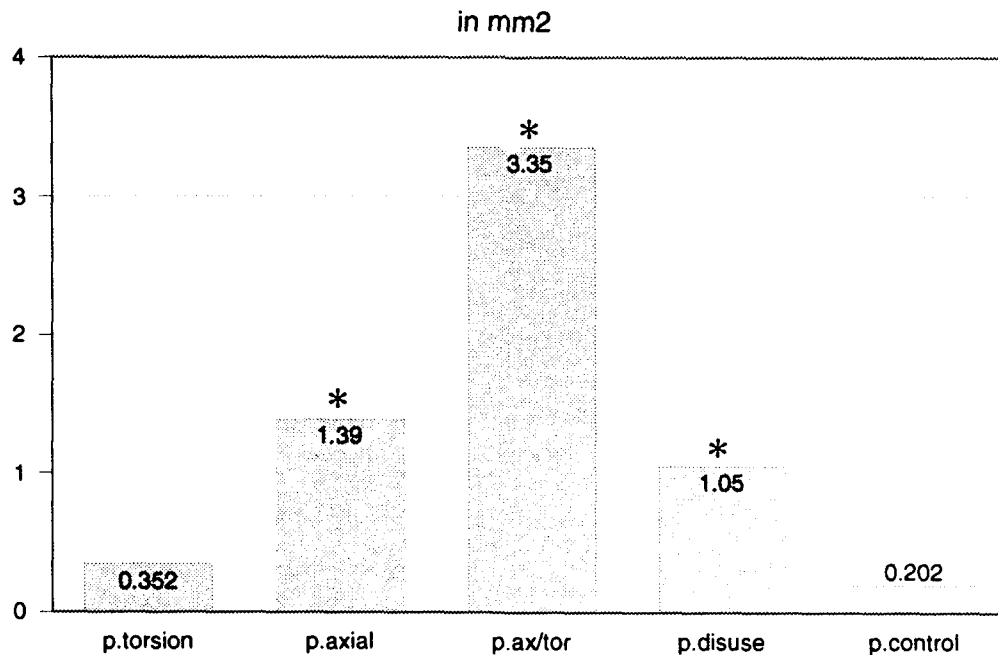


Figure 13. Mean total area of intracortical porosis, in mm<sup>2</sup>, for each of the experimental groups. Statistical differences from control are identified with an asterisk. Note torsional loading did not increase porotic area.

## Number of intracortical porosities

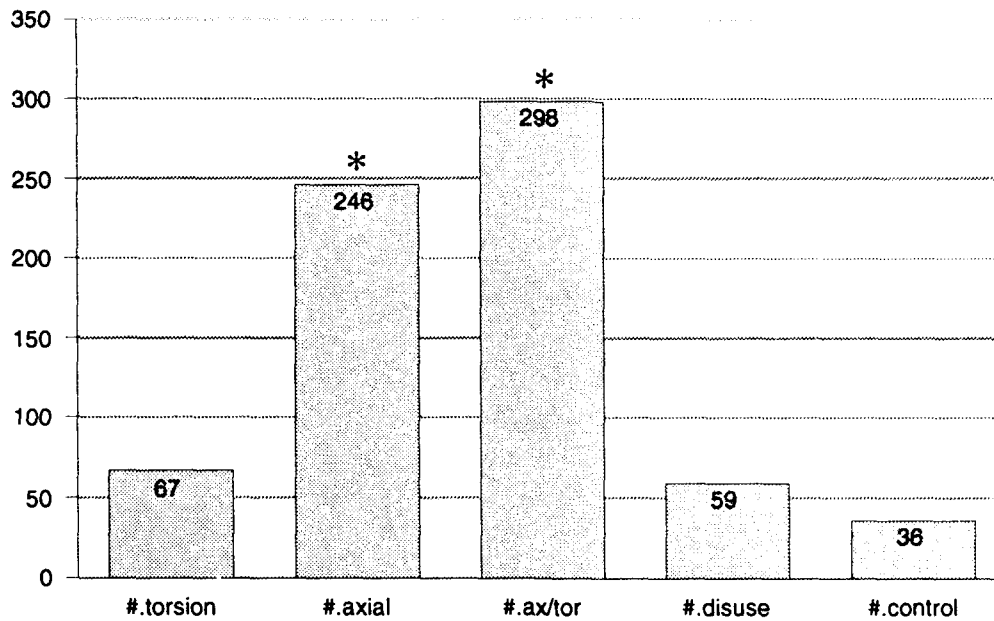


Figure 14. Mean number of intracortical porosities for each of the experimental groups. Statistical differences for control are identified with an asterisk. Note only the two axial conditions caused a difference.

## Total area of midshaft cross-section

in mm<sup>2</sup>

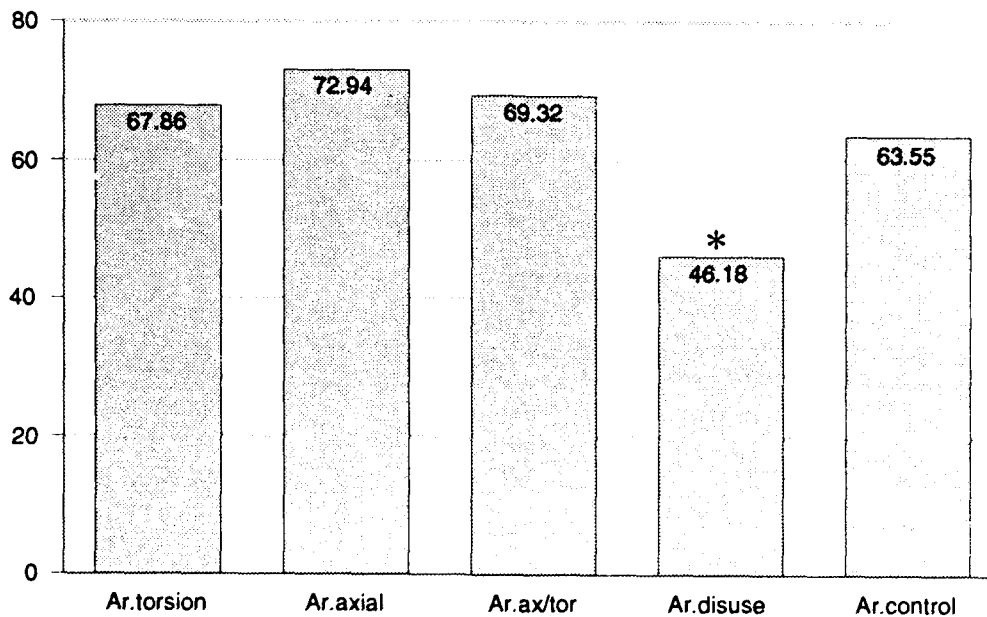


Figure 15. Mean total area of midshaft cross sections. Statistical differences from control are identified with an asterisk. Note only disuse is different, suggesting that the modeling (new bone formation) response is cycle independent.

## Sector analysis of area of porosis

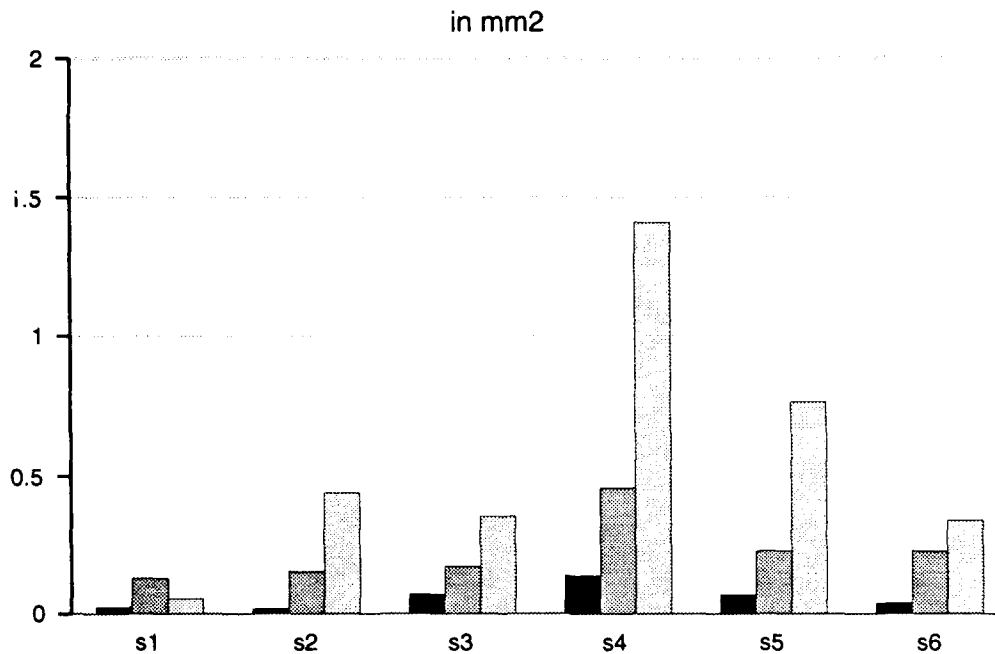


Figure 16. Sector by sector analysis of mean area of porosis, for each of the three experimental groups. Torsion is given as the black bars, axial is the dark shade, and axial/torsion is the light shade. In each case, the greatest degree of activity occurred in sector 4. Indeed, sector 4 was significantly different than many of the other sectors. Interestingly, this is also the area of lowest strain energy density.

## Sector analysis of number of poroses

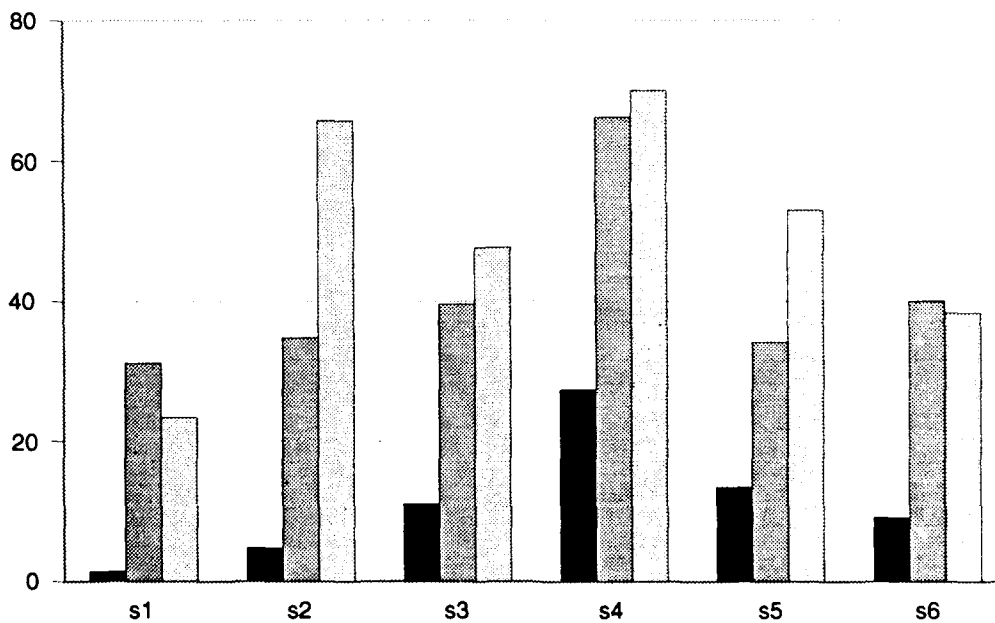


Figure 17. Sector by sector analysis of number of porotic events. In both the torsion (black bar) and axial (dark shaded) conditions, sector 4 showed the greatest intracortical activity. In the combined axial torsion (light shade), activity was elevated about the entire cortex.



## Number of porosities in sector 4

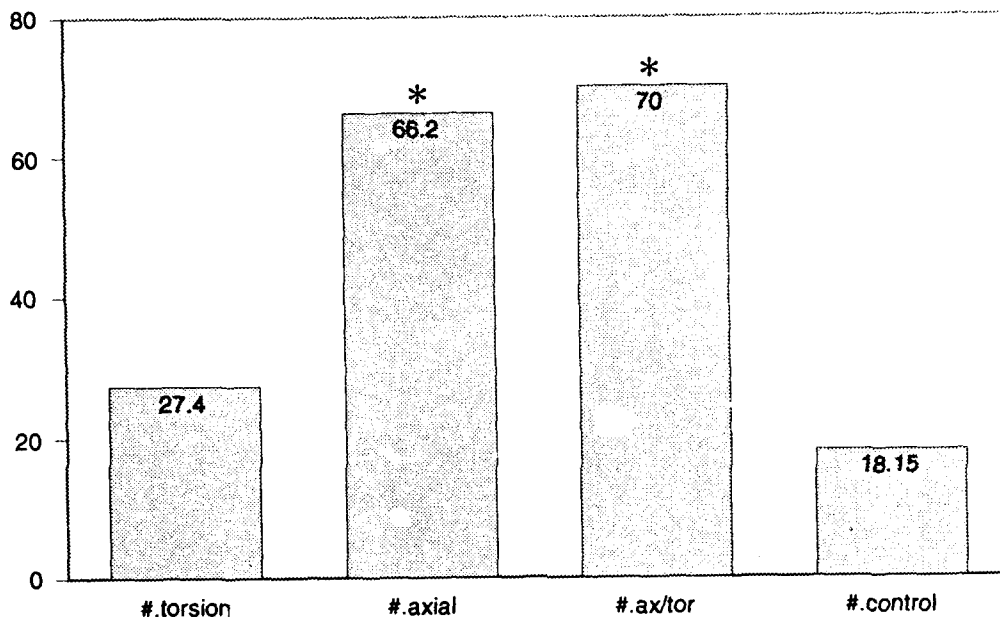


Figure 18. Analysis of porotic activity in sector 4, showing significant differences (\*) between the axial conditions and both torsion and control.

## Area of porosities in sector 4

in mm<sup>2</sup>

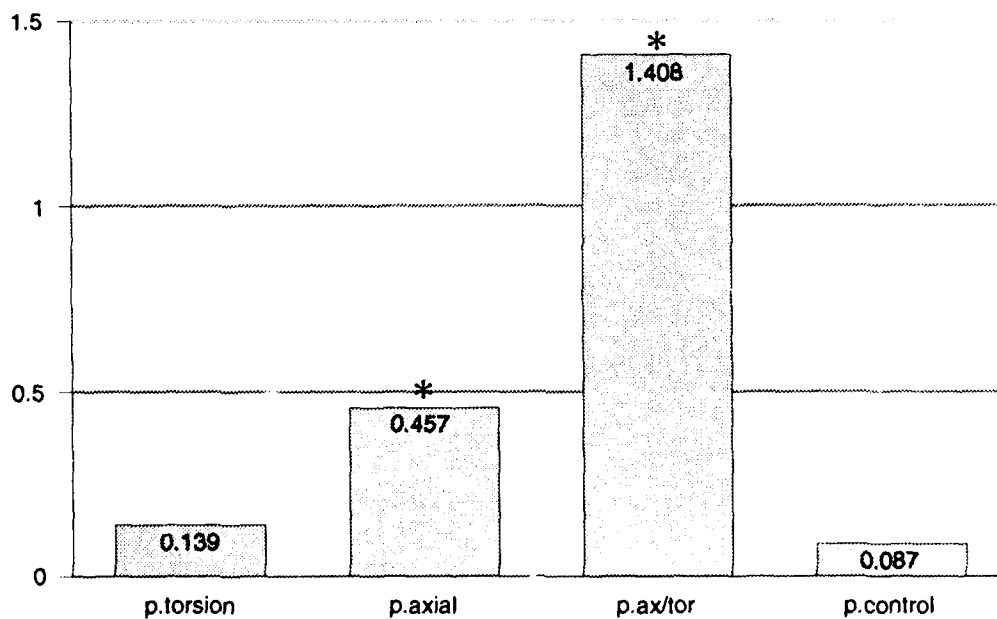


Figure 19. Analysis of area of porosis, in mm<sup>2</sup>, occurring in sector 4 for each of the experimental groups and control. The area of bone lost in this sector is significantly elevated in both axial conditions, while torsion minimizes turnover.

### Discussion

The etiology of the stress fracture condition has been considered previously to be the result of fatigue (Markey 1987; Carter et al. 1981a; Burr et al. 1985). As in the breaking of a paper clip by repeated bending, the stress fracture lesion in the bone cortex has been thought to be generated by accumulation of fatigue microdamage. However, the controlled loading environment made possible by the avian preparation, and corroborated by the correlation of the equine lesion to its functional milieu, emphasizes that the most extensive and demonstrable bone defects associated with excessive repetitions of cyclic loading are not those resulting from an actual "fracture" across the material, but rather a large area of rarefaction, resulting from cellular resorption, which inevitably leads to both pain and structural failure.

As importantly, the lesions produced by loading the avian model do not occur in the area of the cortex subjected to the highest strains, but rather, these lesions occur predominantly in the area of the bone where the strain energy density, as well as normal and shear strains, are least. Transposition of the strain gage data, derived from the horse metacarpal even following metabolic fatigue, demonstrates that naturally occurring stress fractures will also occur in the region of lowest strain history. Extrapolation to the human (an exercise supported by the cross-species similarities evident in the pathology), would suggest that the human condition is also a result of an adaptive response to some aspect of cyclic loading, and is not dependent on microdamage.

In both the natural and the artificially induced lesions, the most remarkable event is not whether there is new bone deposited on the surface (an event that surely does not cause the bone to fracture), rather the elevated and somewhat focalized porosities occurring *within* the cortex. Indeed, it would be the increased loss of bone within the cortex that would compromise the bone's structural integrity and increase the bone's risk of fracture. In the clinical setting, the stress fracture lesion is commonly characterized by a defect of poorly mineralized intracortical bone stretching from one surface of the original cortex to the other. As demonstrated by microradiography, the lesion is not a distinct crack, but rather a large area of rarefaction defined by substantial intracortical remodelling. Considering the areas of high porosity within the cortex and that they occur at the area of least strain, it is clear that this "stress fracture" response should not be considered a "failure of the material", but rather an adaptive remodelling response of the tissue to some cycle dependent aspect of the strain milieu, the *consequence* of which is the "stress fracture" lesion. The resorption of the cortex (and the decrease in effective load bearing area) are thus more likely to be a biologically driven, cycle dependent remodelling response within the bone "tissue," rather than a strain engendered fracture of the bone "material" due to fatigue.

Interestingly, none of the three applied stimuli, axial, torsion nor axial plus torsion, stimulated sufficient new bone formation to make them statistically different from control. Only disuse, in and of itself, caused substantial changes via endosteal resorption and intracortical porosis to be identified as a stimulus strong enough to cause overall differences in area. As these results demonstrate that relatively low amplitudes of mechanical stimuli (1000 microstrain) were not sufficient to stimulate new bone, the mechanical signal that controls "modeling" (new bone at the surfaces) has not passed a "threshold". This supports

the observations of Rubin and Lanyon, 1985, which suggests that 1000 microstrain, even when applied for only 100 cycles per day, is a sufficient "background stimulus" to control bone modeling.

The axial and axial plus torsion stimuli both caused sufficient intracortical resorption to be different from control. As we strongly believe the intracortical poroses to be the critical factor in symptomatic stress fractures, these stimuli must be viewed as deleterious to the bone tissue. Interestingly, torsion, in and of itself, did not elevate either area of intracortical porosis nor number of poroses. This is extremely intriguing, as it would appear that 5000 cycles per day of this relatively low torsional regimen is sufficient to retain the *status quo*, both at the surface and within the cortex. Both axial conditions caused substantial intracortical porosis, yet torsion did not, suggesting that the cell population responsible for the control of remodeling (intracortical turnover) can differentiate between these two types of strain (shear vs. normal). Even though substantial intracortical events occurred, in no load condition did any significant surface activity (modeling) occur. This suggests that the signals that control modeling (surface activity) and remodeling (intracortical activity and resorption) are distinct, and certainly not coupled.

The size of the intracortical events (area of porosis/number of poroses) were essentially identical in the control, torsion and axial groups. However the area of the average event doubled in disuse, and tripled in the combined axial/torsion condition. Considering that the combined axial/torsion condition caused several greenstick fractures to occur, it would appear that the size of the porotic event is a strong indicator of the bone's structural integrity. While many small events not necessarily jeopardize the structure, increasing this porosity puts the structure at grave risk. Therefore, any loading condition (disuse or redundant activity followed by diverse activity) will amplify the potential for a catastrophic loading event.

The number of intracortical porosities increased significantly in both axial conditions. However, neither disuse nor torsion caused any significant change over control. These data suggest that the axial condition, in some unknown way, "actively" increases the intracortical turnover. This is in contrast to a condition such as disuse that "passively" elevates resorptive activity. In other words, considering that the area of intracortical porosis was increased by disuse, yet the number of events did not, suggests that the removal of a mechanical stimulus causes those sites already involved in turnover to simply continue to resorb but not couple it to formative (bone replacement) activity. Conversely, in the axial condition, even though the average size of the porotic event was identical to torsion and control, the *number* of events increased by a factor of seven. This suggests that this loading condition caused a dramatic increase in turnover activity, yet the formation and resorption mechanisms remained coupled. That the axial/torsion combined loading increased *both* area lost (x16) and intracortical events (x8) over control suggests that intracortical activity is again "actively" elevated. These data also demonstrate that the formation and resorption events have again become uncoupled. It is this combined loading case, with elevated resorption uncoupled to formation, that is potentially the most devastating to the structure of the skeleton.

The daily regimen of each loading conditions totalled 5000 cycles per day. Importantly, identical loading intensities, but applied for 100 cycles per day did not elevate any intracortical response (Rubin and Lanyon 1985). As described above, neither the 100 nor 5000 cycle per day regimen stimulated any new bone formation. This demonstrates that the modeling response is cycle independent. However, that *both* 5000 cycle per day axial conditions elevated intracortical activity, suggests that the intracortical remodeling response is cycle dependent. Therefore, if a mechanical stimulus has the *potential* to elevate intracortical activity (i.e. torsion does not), it must surpass some cycle dependent threshold to initiate this response. We have identified a critical component of a stress fracture is elevated intracortical remodeling. Therefore, cycle number is a key determinant in controlling the stress fracture response.

Each of the three loading conditions had peak strains of 1000 microstrain. Indeed, the peak strain energy density in each case was identical. The principal difference between the types of loading, axial vs. torsion, is the manner in which the bone is loaded. In the axial case, the eccentric axial loading causes strain due to bending to occur in the bone. This creates a condition in which one area of the cortex is subject to tension, and one area is subject to compression. This also means that an area of the cortex becomes the neutral axis, an area subject to zero normal strain. This is in stark contrast to the torsional load condition, which creates a somewhat uniform distribution of strain about the bone; there is no distinct area of peak strain, and no area of zero strain. In the sector by sector analysis, sector 4 in the axial condition showed elevated intracortical responses in each case, i.e. the greatest area of intracortical activity was sector 4. Torsion, on the other hand, showed no sector by sector variation to control, nor across sectors. As we are defining stress fractures as increased intracortical activity, sector 4 is certainly the site specific section of bone at greatest risk of failure. However, it is critical to point out that sector 4 is also the area of least strain energy density in the axial loading conditions.

These experiments demonstrate that high cycle numbers of axial loading conditions, even at low strain amplitudes, will initiate the stress fracture response. Conversely, torsional loads essentially retain the *status quo*. This demonstrates two critical components of bone cellular activity; that the cell population can differentiate between normal and shear strain, and that modeling (surface) and remodeling (intracortical) activity are uncoupled. That frank fractures occurred by combining axial and torsional loading suggests that the structural integrity of the bone is first compromised by the intracortical porosis stimulated by axial conditions, and subsequently fails when subject to torsional loading. As the modulus (stiffness) and strength of bone in shear are a fraction of longitudinal modulus and strength, that it fails in torsion is not surprising. That it failed only in the combination loading is surprising; by coupling the intracortical porosis with the shear loads (which did not cause the porosis) was catastrophic.

### Conclusions

The data presented in this report are unique. Essentially, the turkey ulna model provides the only means in which specific components of the mechanical milieu can be evaluated. In the study reported here, it is clear that intracortical porosis and elevated intracortical activity are driven by normal strain while shear strain retains a remodeling

equilibrium. It is also clear that modeling and remodeling can be uncoupled, as can formation and resorption within the cortex. Finally, the site most susceptible to the stress fracture lesion, ironically, appears to be the area subject to least strain. That specific components of loading increase the chance that the bone may subsequently fail is indeed the most catastrophic aspect of the stress fracture pathology. That the lesion is in the area of least strain does not mean that the bone will never fail. A single aberrant loading event will exponentially increase the chance of catastrophic failure by subjecting that area of the cortex to a load that, with the porosities, is not able to withstand.

One inescapable problem with all of these results is how to extrapolate this information to the design of training regimens. The data presented here are extremely specific, and it would be difficult to implement them verbatim in a training regimen. What is clear, however, is that high cycle numbers or a redundant activity which generates a specific neutral axis (e.g. long marches) will elevate intracortical activity. As the greatest degree of activity occurs at or around the area of least strain energy density demonstrates that the intensity of the activity is not relevant, e.g. long marches are just as likely to elevate activity as long runs. Diverse activity, or activities that do not focalize low areas of strain energy density to a single sight, will not initiate the stress fracture lesion. Therefore, activities such as an obstacle course very likely will not elevate remodeling activity. However, training regimes which combine high cycle numbers of activities which focalize low strain energy density, followed by diverse activity, is potentially catastrophic. The redundant activity elevates site specific intracortical porosity, while the diverse activity increases the chance that this porotic area will be subject to strains which the structure cannot withstand.

### References

- Bain, S.D. & Rubin, C.T. (1990): Temporal nature of osteoclast resorption in response to disuse. *J Bone Min. Res.* 5(S2):217.
- Baron, R., Vignery, A. & Horowitz, M. (1983): Lymphocytes, macrophages and the regulation of bone remodeling. In: *Bone and Mineral Research*. ed. W.A. Peck. El Sevier, Amsterdam. v2:175-243.
- Bensel, C.K. (1986): The effects of tropical and leather combat boots on lower extremity disorders among U.S. Marine Corps. recruits. U.S. Army Natick Res. & Devmt. Cmd. Report 76-49-CEMEL.
- Bernstein, A. & Stone, J.R. (1944): March fracture: A report of three hundred and seven cases and a new method of treatment. *J. Bone and Joint Surg.* 26:743-750.
- Brand, R. & Rubin, C. (1988): Fracture Healing. In: *The Scientific Basis of Orthopaedics*. eds. J. Albright & R. Brand. Appleton Century Crofts Publishers, N.Y., N.Y. 11:325-345
- Brown, T.D., Pedersen, D.R., Gray, M.L., Brand, R.A. & Rubin, C.T. (1990): Identification of mechanical parameters initiating periosteal remodeling: A complimentary experimental and analytic approach. *J. Biomech.* 23:893-905.
- Brudvig, T.J.S., Gudger, T.D. & Obermeyer, L. (1983): Stress fractures in 295 trainees: A

one-year study of incidence as related to age, sex, and race. *Mil. Med.* 148:666-667.

Burr, D.B., Martin, R.B., Schaffer, M.B. & Radin, E.L. (1985): Bone remodeling in response to in vivo fatigue microdamage. *J. Biomech.* 1B:189-200.

Carter, D.R., Harris, W.H., Vasu, R. & Caler, W.E. (1981a): The mechanical and biological response of cortical bone to in vivo strain histories. *Mechanical properties of bone; AMD* 45:81-92.

Chamay, A., & Tschantz, P. (1972): Mechanical influence in bone remodeling: Experimental research on Wolff's Law. *J. Biomech.* 5:173-180.

Chisin, R., Milgrom, C., Giladi, M., Stein, M., Margulies, J., & Kashtan, H. (1987): Clinical significance of nonfocal scintigraphic findings in suspected tibial stress fractures. *Clin. Orthop. Rel. Res.* 220:200-205.

Daffner, R.H.: Stress fractures (1978): Current concepts. *Skeletal Radiol.* 2:221-229.

Duker, R.P. (1982): Memorandum for Deputy Commanding General: Stress fracture test results. Headquarters U.S. Army Training Center at Fort Jackson.

Fiedl, K.E., Nuovo, J.A., Patience, T.H., & Dettori, J.R. (1992): Factors associated with stress fracture in young army women: Indications for further research. *Military Med.* 157:334-338.

Floyd, W.N., Butler, J.E., Clanton, T., Kim, E.E., & Pjura, G. (1987): Roentgenologic diagnosis of stress fractures and stress reactions. *South Med. J.* 80:433-439.

Frost, H.L. (1960): Presence of microscopic cracks in vivo in bone. *Henry Ford Hospital Medical Bull.*, Vol. 8.

Gardner, L., Dziados, J.E., Jones, B.H., Brundage, J.F., Harris, J.M., Sullivan, R., & Grill, R. (1988): Prevention of lower extremity stress fractures: A controlled trial of a shock absorbent insole. *Am. J. Public Health* 78:1563-1567.

Giladi, M., Ahronson, Z., Stein, M., Danon, Y.L., & Milgrom, C. (1985): Unusual distribution and onset of stress fractures in soldiers. *Clin. Orthop. Rel. Res.* 192:142-146.

Goldfarb, C. Richard (1988): Interpretation and classification of bone scintigraphic findings in stress fractures. *J. Nuclear Med.* 29:1150-1151.

Gray, M. & Rubin, C.T. (1987): Distribution of strain magnitude in the cannon bone of the horse. *11th Amer. Soc. Biomech.* 11:287.

Greaney, R., Gerber, F., Laughlin, R., Kmet, J., Metz, C., Kilcheski, T., Rau, B., & Silverman, E. (1983): Distribution and natural history of stress fractures in U.S. Marine

recruits. *Radiology* 146:339-346

Gross, T., McLeod, K.J., & Rubin, C.T. (1992): Characterizing bone strain distributions in vivo using three triple rosette strain gages. *J. Biomechanics* (in press).

Hayes, W.C. & Snyder, B. (1981): Toward a quantitative formulation of Wolff's Law in trabecular bone. *ASME publ. AMD, Cowin, S. (ed)* 45:43-68.

Jones, B.H., Harris, J.M., Vinh, T.N. & Rubin, C. (1989): Exercise-induced stress fractures and stress reactions of bone: Epidemiology, etiology and classification. *Exercise and Sport Sciences Reviews* 11:379-422.

Koblik, P.D., Hornof, W.J. & Seeherman, H.J. (1986): Scintigraphic appearance of stress-induced trauma of the dorsal cortex of the third metacarpal bone in racing thoroughbred horses: 121 cases. *J. Amer. Vet. Med. Assoc.* 192:390-395.

Lanyon, L.E. & Rubin, C.T. (1984): Static vs. dynamic loads as an influence on bone remodeling. *J. Biomech.* 17:897-906.

Leichter, I., Simkin, A., Margulies, J.Y., Bivas, A., Steinberg, R., Giladi, M. & Milgrom, C. (1989): Gain in mass density of bone following strenuous physical activity. *J. Orthop. Res.* 7:86-90.

Leveton, A.L. (1946): March (fatigue) fractures of the long bones of the lower extremities. *Am. J. Surg.* 71:222-232.

Maclaren, D.P.M., Gibson, H., Parry-Billings, M., & Edwards, R.H.T. (1989): A review of metabolic and physiological factors in fatigue. *Exercise and Sport Sciences Reviews.* 17(2):29-66.

Margulies, J., & Altan, H. (1984): Negative bone scans in impending tibial stress fractures. A report of three cases. *Am. J. Sports Med.* 12:488-491. Page 1

Markey, K.L. (1987): Stress fractures. *Clin. Sports Med.* 6:405-425.

Matheson, G.O., Clement, D.B., McKenzie, D.C., Tauton, J.E., Loyd-Smith, D.R., & Macintyre, J.G. (1987): Scintigraphic uptake of 99m Tc at non-painful sites in athletes with stress fractures. *Sports Med.* 4:65-75.

McBryde, A.M. (1985): Stress fractures in runners. *Clin. Sports Med.* 4:737-752.

Milgrom, C., Giladi, M., Chisin, R., & Dizian, R. (1985a): The long term follow-up of soldiers with stress fractures. *Am. J. Sports Med.* 13:398-400.

Milgrom, C., Giladi, M., Stein, H., Kashton, H., Margulies, J., Chisin, R., Steinberg, R., & Aharonson, Z. (1985b): Stress fractures in military recruits: A prospective study showing an

unusually high incidence. *J. Bone and Joint Surg.* 67B:732-735.

Milgrom, C., Chisin, R., Giladi, M., Stein, M., Kashtan, H., Margulies, J. & Atlan H. (1985c): Multiple stress fractures. *Clin. Orthop. Rel. Res.* 192:174-179.

Miller, S.G., Shupe, V.G., Redd, E.H., Miller, M.A., & Omura, T.H. (1986): Changes on bone mineral and bone formation rates during pregnancy and lactation in rats. *Bone* 7:283.

Nunamaker, D.M., Butterweck, D.M., & Black, J. (1987): Fatigue fractures in thoroughbred racehorses: Relationship with age and strain. *Trans. 33rd Orthop. Res. Soc.* 12:72.

Nussbaum, A.R., Treves, S. Ted & Micheli, L. (1988): Bone stress lesions in ballet dancers: Scintigraphic assessment. *Amer. J. Radiology* 150:851-855.

Parfitt, A.M., Drezner, M.K., Glorieux, F.H., Kanis, J.A., Malluche, H., Meunier, P.J., Ott, S.M., & Recker, R.R. (1987): Bone histomorphometry: Standardization of nomenclature, symbols, and units. *J. Bone Min. Res.* 2:595.

Protzman, R.R. & Griffis, C.G. (1977): Stress fractures in men and women undergoing military training. *J. Bone and Joint Surg.* 59A:825.

Recker, R. (1983): *Bone Histomorphometry: Techniques and interpretation.* CRC Press, Inc., Boca Raton, FL.

Rubin, C. & Lanyon, L. (1982): Limb mechanics as a function of speed and gait: A study of functional strains in the radius and tibia of horse and dog. *J. Exp. Biol.* 101:187-211.

Rubin, C.T. & Lanyon, L.E. (1984): Regulation of bone formation by applied dynamic loads. *J. Bone and Joint Surg.* 66A:397-402.

Rubin, C.T., Harris, J., Jones, B., Ernst, H. & Lanyon, L.E. (1985): Stress fractures: The remodeling response to excessive repetitive loading. *Trans. 30th Ortho. Res. Soc.* 9:303.

Rubin, C.T. & Lanyon, L.E. (1985): Regulation of bone mass by mechanical strain magnitude. *Calc. Tissue Intl.* 37:411-417.

Rubin, C.T., Harris, J.M., Sweet, C., Jones, B. & Lanyon, L.E. (1985): Stress fractures: An alternative etiology. *Trans. 5th Eur. Soc. Biomech.* p. 230.

Rubin, C.T., Pratt, G.W., Porter, A.L., Lanyon, L.E. & Poss, R. (1987a): The use of ultrasound in vivo to determine acute change in the mechanical properties of bone following intense physical activity. *J. Biomechanics* 20(7):723-727.

Rubin, C.T., & Lanyon, L.E. (1987): Osteoregulatory nature of mechanical stimuli: Function as a determinant for adaptive remodeling in bone. *J. Orthop. Res.* 5:300-310.



- Rubin, C.T. & Hausman, M.R. (1988): The cellular basis of Wolff's Law: Transduction of physical stimuli to skeletal adaptation. *Rheum. Dis. Clin. North Amer.* 14(3):503-517.
- Rubin, C.T. & Bain, S.D. (1989): Suppression of the osteogenic response in the aging skeleton. *Proc. 11th Amer. Soc. for Bone and Min. Res.* 4:S374.
- Rubin, C.T., McLeod, K.J. & Bain, S.D. (1989a): Functional strains and cortical bone adaptation: Epigenetic assurance of skeletal integrity. *J. Biomech.* 23(S1):43-54.
- Rubin, C., Vasu, R., Tashman, J., Seeherman, H., & McLeod, K. (1989b): The non-uniform distribution of shear strains in functionally loaded bone: Implications for a complex mechanical milieu. *Trans. 35th Ortho. Res. Soc.* 14:313
- Rubin, C., Vasu, R., McLeod, K. & Seeherman, H. (1989c): The correlation of metabolic fatigue to changes in the skeleton's mechanical milieu. *Amer. Soc. Biomech.* 13:246-247.
- Schmidt, T.J., Gudger, T.D. & Obermeyer, L. (1982): 339 Stress fractures in 285 trainees: A one year study of incidence as related to age, sex and race. *Physical Therapy Clinic-Noble Army Hospital N/A*, 1-5.
- Scully, T.J., & Besterman, G. (1982): Stress fracture: A preventable injury. *Mil. Med.* 147:285-287.
- Swissa, A., Milgrom, C., Giladi, M., Kashtan, H., Stein, M., Margulies, J., Chisin, R., & Aharonson, Z. (1989): The effect of pretraining sports activity on the incidence of stress fractures among military recruits: A prospective study. *Clin. Orth. Rel. Res.* 245: 256-260.
- Uthoff, H.K. & Jaworski, Z.F. (1985): Periosteal stress induced reactions resembling stress fractures. *Clin. Orthop. Rel. Res.* 199:284-291.
- Zwas, S.T., Elkanovitch, R., & Frank, G. (1987): Interpretation and classification of bone scintigraphic findings in stress fractures. *J. Nucl. Med.* 28:452-457.
- Zwas, S.T., Rupani, H.D., Maurer, A.H., Matin, P., Holder, L., Brady, D.M., Viitasalo, J.T., Slocum, D.B. & Michael, R.D. (1988): Interpretation and classification of bone scintigraphic findings in stress fractures. *J. Nucl. Med.* 29(6):1150-1151.